Copyright Warning & Restrictions

The copyright law of the United States (Title 17, United States Code) governs the making of photocopies or other reproductions of copyrighted material.

Under certain conditions specified in the law, libraries and archives are authorized to furnish a photocopy or other reproduction. One of these specified conditions is that the photocopy or reproduction is not to be "used for any purpose other than private study, scholarship, or research." If a, user makes a request for, or later uses, a photocopy or reproduction for purposes in excess of "fair use" that user may be liable for copyright infringement,

This institution reserves the right to refuse to accept a copying order if, in its judgment, fulfillment of the order would involve violation of copyright law.

Please Note: The author retains the copyright while the New Jersey Institute of Technology reserves the right to distribute this thesis or dissertation

Printing note: If you do not wish to print this page, then select "Pages from: first page # to: last page #" on the print dialog screen

NJIT
New Jersey's Science & Technology University

The Van Houten library has removed some of the personal information and all signatures from the approval page and biographical sketches of theses and dissertations in order to protect the identity of NJIT graduates and faculty.

ABSTRACT

SILICON OPTICAL FIBER SENSOR

by
Jian Pan

A novel optical fiber pressure sensor based on a micromachined thin silicon diaphragm is proposed. Detail descriptions of the sensor structure, modulation principle and fabrication process are given.

The device operates on the following principle: Pressure deflects a silicon diaphragm which moves the output end of a light source fiber. The emitted light intensity is picked up and shared by two receiving fibers placed side by side. The variation of the intensity ratio in the receiving fibers caused by the relative motion of the emitting fiber can be easily converted to a linear signal versus the deflection of the silicon diaphragm. This ratio is independent of the light source intensity so that fluctuations of a light source is automatically compensated. Having advantages of both a silicon sensor and a optical fiber sensor, such as compactness and immunity to electromagnetic field, the sensor works with good linearity and sensitivity.

SILICON OPTICAL FIBER PRESSURE SENSOR

by
Jian Pan

Robert W. Van Houten Library
New Jersey Institute of Technology

A Thesis
Submitted to the Faculty of
New Jersey Institute of Technology
in Partial Fulfillment of the Requirements for the Degree of
Master of Science in Applied Physics

Department of Physics

January 1995

APPROVAL PAGE

SILICON OPTICAL FIBER PRESSURE SENSOR

Jian Pan

Dr. John C. Hensel, Thesis Advisor — Date
Distinguished Research Professor in Applied Physics, NJIT

Dr. Ken K. Chin, Committee Member — Date
Professor of Physics
Director of Joint NJIT/Rutgers(Newark) Applied Physics
M.S./Ph.D. Graduate Program, NJIT

Dr. Nuggehalli M. Ravindra, Committee Member — Date
Associate Professor of Physics, NJIT

BIOGRAPHICAL SKETCH

Author: Jian Pan

Degree: Master of Science in Applied Physics

Date: January 1995

Undergraduate and Graduate Education

- Master of Science in Applied Physics,
  New Jersey Institute of Technology,
  Newark, New Jersey, 1995

- Bachelor of Science in Applied Physics,
  Dalian University of Technology,
  Dalian, China, 1985

Major: Applied Physics

This thesis is dedicated to my wife

ACKNOWLEDGMENT

The author wishes to express his sincere gratitude to his advisor, Dr. John Hensel, for his guidance and encouragement throughout this research.

The author also wishes to thank his committee members, Dr. Ken K. Chin and Dr. Nuggehalli M. Ravindra, not only for their efforts in reviewing and evaluation of this thesis, but also for their valuable help and suggestions in the preparation of the thesis.

The author would also like to thank to Michael Grieco in Microelectronics Center of NJIT for his help in wafer processing.

The author is very grateful to his friends, Deguang Zhu, Zhenyu Ma, Xinde Wang, and Professor Yuan Yan for their continuous assistance and encouragement in this research.

TABLES OF CONTENTS

Chapter Page

1 INTRODUCTION ... 1

1.1 Silicon Pressure Sensor ... 1

1.2 Silicon Optical Fiber Sensor ... 3

2 SENSOR STRUCTURE AND PRINCIPLE ... 6

2.1 Sensor Structure and Sensing Mechanism ... 6

2.2 Deflection of Silicon Diaphragm ... 8

2.2.1 Introduction ... 8

2.2.2 Flat Circular Diaphragm and Flat Square Diaphragm ... 9

2.2.3 Non-planar Diaphragm ... 9

2.2.3.1 Bossed Circular Diaphragm ... 10

2.2.3.2 Corrugated Circular Diaphragm ... 10

2.2.3.3 Bossed and Corrugated Circular Diaphragm ... 12

2.2.3.4 Non-planar Square Diaphragm ... 13

2.3 Principles of Modulation and Compensation ... 15

3 FABRICATION ... 19

3.1 Silicon Micromachining ... 19

3.2 Mask Design and Making ... 21

3.3 Wafer Processing ... 24

3.3.1 Wafer Cleaning and Oxidation ... 24

3.3.2 Photolithography ... 25

3.3.3 Oxide Etch ... 25

3.4 Anisotropic Etching of Crystalline Silicon ... 25

3.4.1 Introduction ... 25

3.4.2 Etchants for Anisotropic Etching of Silicon ... 27

TABLES OF CONTENTS
(Continued)

Chapter **Page**

3.4.3 Etching Process 27

3.4 Assembly and Packaging 29

4 SIGNAL PROCESSING 30

4.1 An Overview of the Sensor 30

4.2 Light Source 32

4.3 Light Detection 32

4.3 Signal Amplification and Processing 32

5 EXPERIMENTS 35

5.1 Experimental Set-up 35

5.2 Measurement of Characteristics of Sensor 36

5.2.1 Measurement of Deflection and Response Characteristics 36

5.2.2 Comparison of Different Light Source 38

5.2.3 Characteristics of Light Intensity Compensation 39

5.2.4 Effect of End Distance Between Source Fiber and Receiving Fiber 39

5.3 Discussion of Non-linearity and Application Limitations 41

6 CONCLUSION 44

APPENDIX A Signal Amplification and Processing Circuit 45

APPENDIX B Data Acquisition and Processing Program 46

APPENDIX C Experimental Data of Sensor Testing 48

REFERENCES 49

LIST OF TABLES

Table **Page**

Table C.1 Experimental Data 48

LIST OF FIGURES

Figure		Page
1.1	Silicon Piezoresistive Pressure Sensor	2
1.2	Silicon Capacitive Pressure Sensor	2
1.3	Light Modulation in Passive Fiber-optic Silicon Sensors	4
1.4	Modulating Principle of Silicon Optical Fiber Sensor	5
2.1	Structure of Silicon Optical Fiber Pressure Sensor	7
2.2	Load-deflection Characteristics of Flat and Corrugated Diaphragm	11
2.3	Comparison of Flat and Corrugated Diaphragm Response	13
2.4	Measured and FEA Calculated Diaphragm Deflection versus Pressure with a Boss and Corrugations Used for Low-pressure Sensor	13
2.5	Deflection vs. Pressure for Various Square Diaphragm Structures	14
2.6	Multimode Optical Fiber in Radially Symmetric Coordinates	15
2.7	Light Source Fiber and Receiving Fibers in Rectangular Coordinates	17
3.1	Fabrication Process Sequence for Pressure Sensing Silicon Diaphragm	20
3.2	Figures for Mask Design	22
3.3	Optical Fibers in V-grooves	23
3.4	Mask Created by SLR Camera	24
3.5	Orientation Dependent Etching	26
3.6	Finished Wafer	28
3.7	Modified Mask Design	29
4.1	Schematic Diagram of the Silicon Optical Fiber Pressure Sensor	31
4.2	Block Diagram of Signal Amplification and Processing	33
5.1	Schematic Depiction of the Experimental Set-up for the Testing of Sensor	36
5.2	Output Signal vs. Diaphragm Deflection	37

LIST OF FIGURES
(Continued)

Figure **Page**

5.3 Comparison of Sensor's Characteristics for Different Light Sources....................38

5.4 Characteristics of Light Intensity Compensation 40

5.5 Response Comparison of Different Distances
between Ends of Source Fiber and Receiving Fibers 41

CHAPTER 1

INTRODUCTION

1.1 Silicon Pressure Sensor

With the development of precision silicon micromachining technology, various kinds of silicon sensors have been developed[1]-[10]. Due to their advantages such as compactness, high sensitivity and reliability, these sensors have become more and more important in many areas, including transportation, health care, and industrial process control.

Of all these silicon sensors, the silicon pressure sensor is one of the most important and has been well studied. A lot of types of silicon pressure sensors have been proposed. All these sensors employ the deflection of a thin diaphragm etched in a silicon wafer, but the readout technologies are quite different.

Piezoresistive and capacitive readouts are the most common methods used; resonance and magnetic induction have also been used in some silicon pressure sensors[2]. A prototype silicon piezoresistive pressure sensor is shown in Figure 1.1[1]. It consists of a thin silicon diaphragm as a pressure sensing element and piezoresistive gauge resistors made by impurity diffusing. By connecting the resistors in a bridge circuit and exciting the bridge with electrical power, pressure-to-electric output conversion can be accomplished. Silicon diaphragms can be also used with another pressure-to-electrical transducer employed in capacitive sensors[4], as shown in Figure 1.2. Here, the diaphragm deflection modulates the capacitance of a parallel-plate capacitor. Since the output signals are often processed by circuits integrated on these sensors, the additional circuitry necessary to accomplish calibration is greatly simplified. For this reason these sensors are often called smart sensors[3]. But on the other hand, due to the built-in circuitry, piezoresistive sensors, capacitive sensors and other sensors with built-in circuitry have one main

drawback. They are subject to electromagnetic interference. Besides, most piezoresistive sensors and some capacitive sensors are quite temperature sensitive. Thus, additional thermal compensations are required. This increases the complexity of sensor structures and the cost of manufacturing.

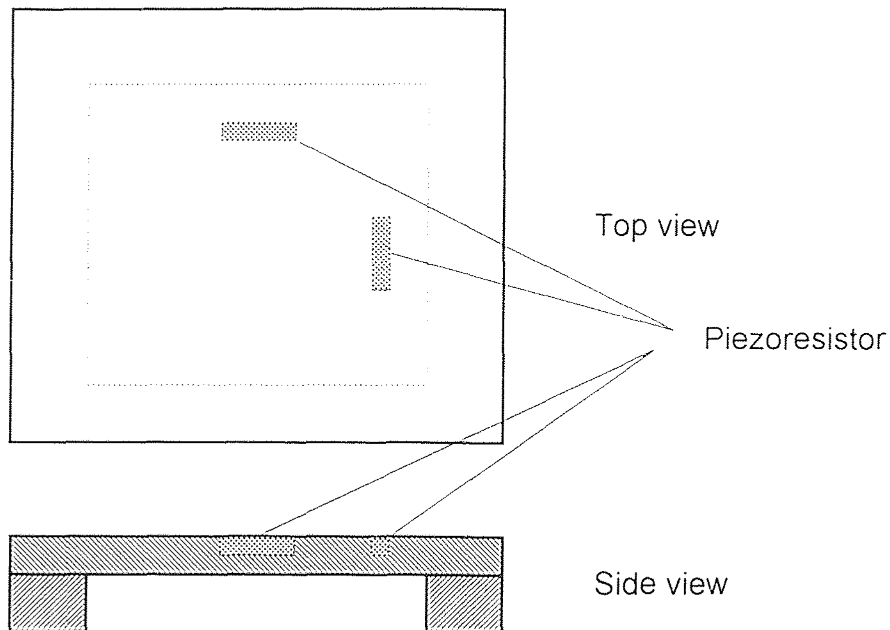

Figure 1.1 Silicon Piezoresistive Pressure Sensor

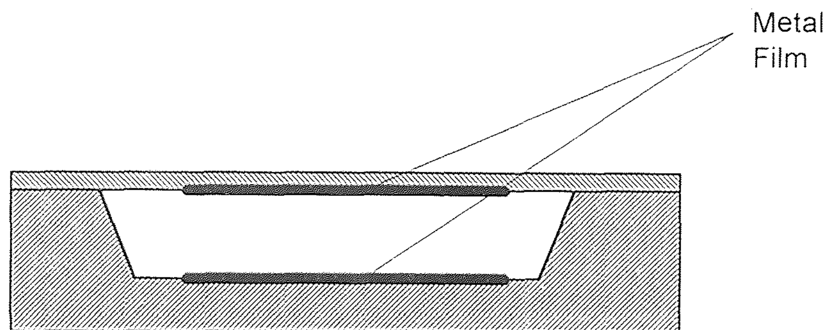

Figure 1.2 Silicon Capacitive Pressure Sensor

1.2 Silicon Optical Fiber Pressure Sensor

Optical fiber sensors (OFS) show great advantages over most conventional sensors:

- good electrical isolation
- immunity to electromagnetic interference
- safety in explosive environments
- suitable for remote sensing
- low temperature effect
- low signal attenuation
- compactness

By combining optical fiber sensing techniques with silicon microengineering, it is possible to fabricate new types of sensors which are ultra compact, highly sensitive, largely unaffected by temperature, immune to electromagnetic interference, and intrinsically safe. Several designs of silicon optical fiber pressure sensors have been proposed in the past few years [8]-[11].

Figure 1.3 shows several designs of silicon optical fiber sensors. In Figures 1.3a-e are intensity modulation type sensors; Figure 1-3f is an interference pattern modulation type, but in this device it is also the intensity of the output pattern that is measured. All these sensors are passive type optical fiber sensors. There are no output electrical signals and no electrical power supply needed.

Some other type silicon optical fiber sensors are hybrids of silicon IC technology, silicon micromachining, and fiber optics[8]. These sensors have the advantages of silicon sensors and some advantages of optical fiber sensors. But some intrinsic disadvantages of integrated silicon sensors still remain.

For the passive optical fiber sensors shown in Figure 1.3, there are also some problems in their applications. The outputs of these sensors are subject to the influence of light source fluctuations or are inherently nonlinear. For good accuracy and stability, some forms of referencing and calibration are needed.

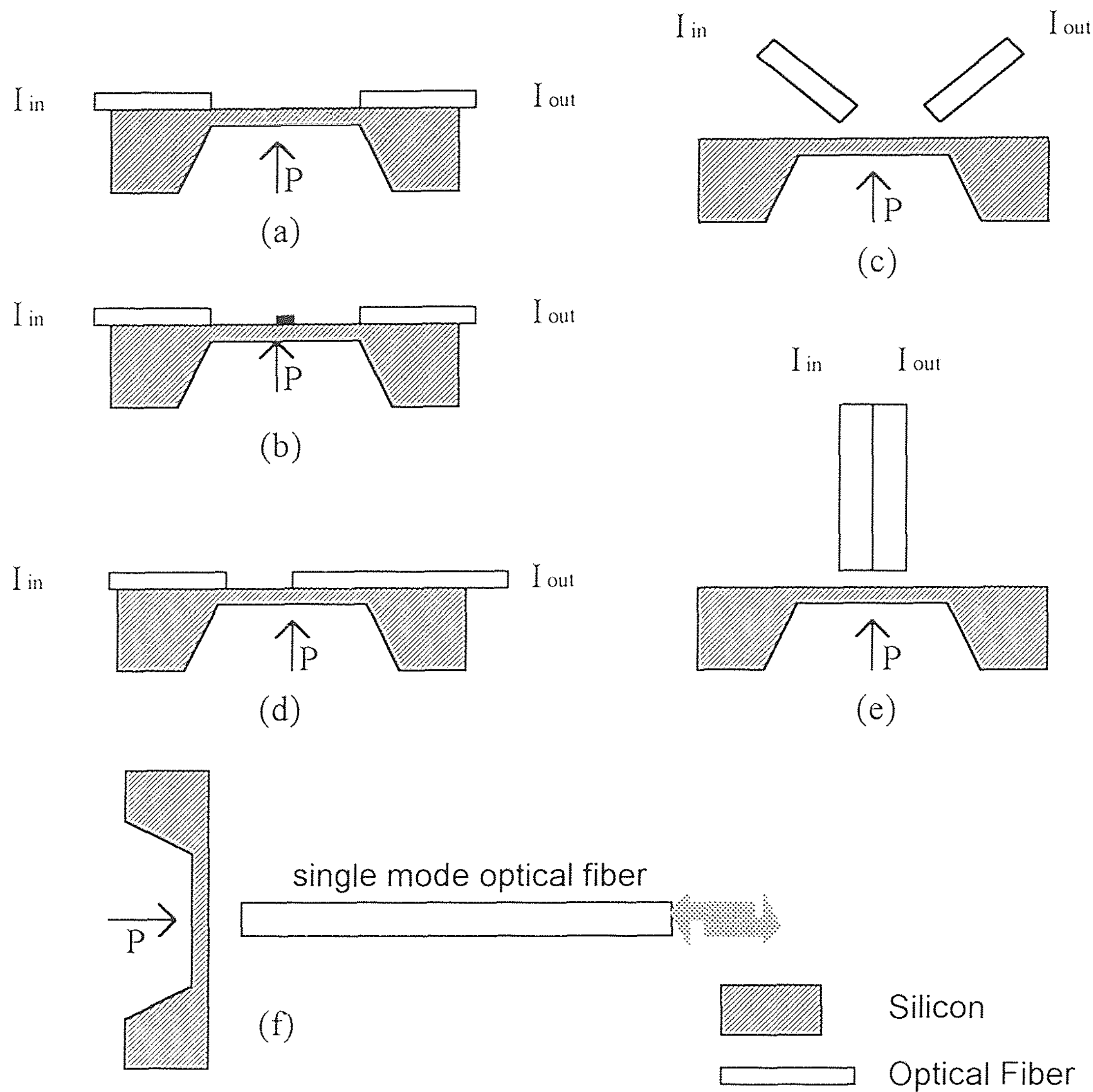

Figure 1.3 Light Modulation in Passive Fiber-optic Silicon Sensors[8]&[9]

In this thesis, a novel silicon optical fiber pressure sensor is described. The structure is quite simple and the fabrication process is relatively easy. The modulation principle is schematically shown in Figure 1.4. Light is emitted from the end of an optical fiber whose position is controlled by a pressure diaphragm. The ratio of light intensities picked up by two side-by-side receiving fibers is thus a function of pressure. The sensor needs no electrical supply. This makes the sensor very useful for remote sensing in a flammable

environment or environment having electromagnetic interference. The sensor's output can be easily converted to a linear signal proportional to the deflection of the silicon diaphragm. Furthermore, the light source fluctuations, which are often the main error source of intensity modulated optical fiber sensors, are automatically compensated.

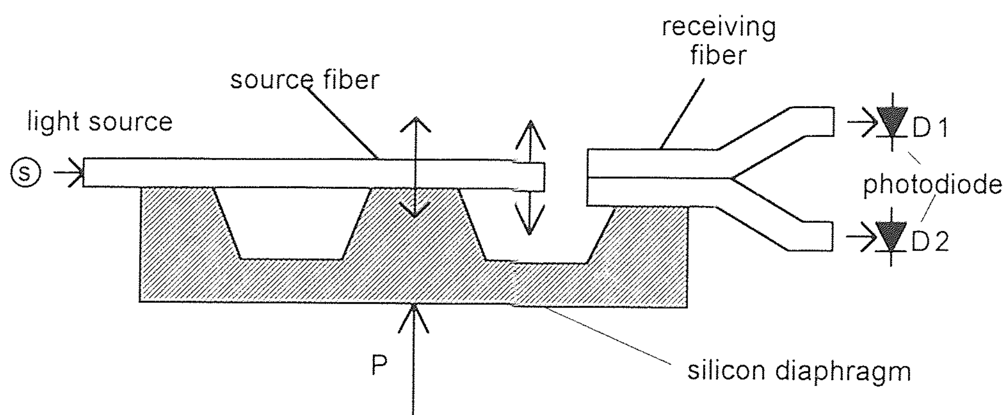

Figure 1.4 Modulation Principle of Silicon Optical Fiber Pressure Sensor

CHAPTER 2

SENSOR STRUCTURE AND PRINCIPLE

2.1 Sensor Structure and Sensing Mechanism

The structure of the sensor is schematically shown in Figure 2.1. It consists of the following parts:

(1) A silicon micromachined die which has a bossed diaphragm for pressure sensing and has V-grooves for optical fiber alignment.

(2) A silicon over pressure protection which has a symmetric structure to the die, except that a small portion of the boss has been etched off.

(3) A multimode optical fiber as light source of the sensor. One end of the fiber is coupled to a laser diode or other light source, the other end is glued in the V-groove in the diaphragm.

(4) Two multimode fibers as light detectors. One end of the twin receiving fibers is facing the output end of the source fiber, the other end is connected to photo diodes or other light detecting devices.

(5) A silicon support.

All these parts are bonded together by epoxy glue.

When there is a pressure imposed on the diaphragm, the diaphragm will be deflected and the output end of the source fiber moves with the diaphragm. Because the source fiber is illuminating the twin receiving fiber, the light intensity received by the twin receiving fibers will also change due to the deflection of the diaphragm. By detecting the output of the twin receiving fibers, the displacement of the light source or the deflection of the diaphragm can be determined[24]. If the relationship between the deflection of the diaphragm and the applied pressure is known and calibrated, the pressure can be determined by detecting the output ratio of the twin receiving fibers.

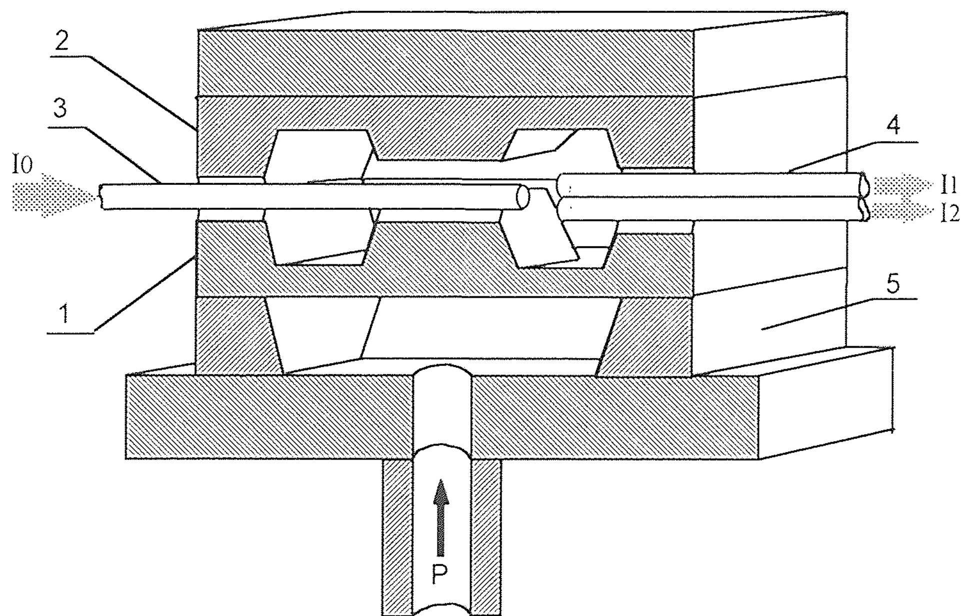

Figure 2.1. Structure of Sensor

1. die with sensing diaphragm
2. over pressure protection
3. light source optical fiber
4. light receiving optical fibers
5. support

2.2 Deflection of Silicon Diaphragms

2.2.1 Introduction

The outstanding mechanical properties of silicon make it ideal as a pressure sensing diaphragm material[12]. Having less mechanical hysteresis is one and possibly the most important advantage of silicon over other materials for pressure sensing applications. In addition, by using the well developed silicon microengineering technology, different structures of silicon with very compact sizes can be created in a precisely controllable and reproducible manner. For these reasons, more and more attention has been paid to silicon sensors, and currently a large variety of silicon pressure sensors are manufactured commercially.

To obtain pressure sensors with good characteristics and optimum the designs, people have made consistent efforts to get the precise load-deflection relations of silicon diaphragms. During the years, a lot of studies and experiments have been conducted on the load-deflection relations of silicon diaphragms with different geometries[13]-[21].

For any diaphragm, regardless of the shape and profile, we can express its load-deflection relation as:

$$\frac{Pa^4}{Eh^4} = A_p\left[\frac{y}{h}\right] + B_p\left[\frac{y}{h}\right]^3 \tag{2.1}$$

where P is applied pressure, y is the center deflection of the diaphragm, a is a dimension parameter of the diaphragm(for a circular diaphragm, a is the radius; for a square diaphragm, a is the half side length), E is Young's modulus, and h *is* the diaphragm thickness. A_p and B_p are called linear and cubic coefficients, respectively. They are constants depending on the profile of the diaphragm and Poisson's ratio ν of the diaphragm material.

2.2.2. Flat Circular Diaphragm and Flat Square Diaphragm

The load-deflection relation of a flat, clamped circular diaphragm is given by [13]:

$$\frac{Pa^4}{Eh^4} = \frac{16}{3\left(1-\nu^2\right)}\left(\frac{y}{h}\right) + \frac{7-\nu}{3(1-\nu)}\left(\frac{y}{h}\right)^3 \tag{2.2}$$

and the load-deflection relation of a flat square diaphragm is[14]

$$\frac{Pa^4}{Eh^4} = \frac{4.20}{\left(1-\nu^2\right)}\left(\frac{y}{h}\right) + \frac{1.58}{(1-\nu)}\left(\frac{y}{h}\right)^3 \tag{2.3}$$

where P, a, E, h and ν are defined as in Equation (2.1). For the same value of a, a circular diaphragm is about 30% stiffer than the square diaphragm for small deflection. The ratio of linear to cubic coefficients of the two diaphragms are nearly equal, this means the non-linearity is similar. For deflections more than 25% of the thickness of the diaphragms, the non-linearity of both diaphragms is significant regardless of the dimensions of the diaphragm.

2.2.3. Non-Planar Diaphragm

To avoid or reduce the non-linearity caused by membrane stresses, which becomes significant for both square and circular diaphragms for large deflection, more elaborate schemes have been proposed to enhance linearity[5][16]-[22]. The most often used method is the employment of a stiffening boss and/or corrugations on a diaphragm. Detail discussions of these non-planar diaphragm are given in the following sections.

2.2.3.1 Bossed Circular Diaphragm

For a circular diaphragm with a center boss the linear term as in Equation (2.1) is dominant for small deflection, the non-linear term is negligible. The center deflection can be expressed as[13]:

$$\left[\frac{Pa^4}{Eh^4}\right] = A_p \frac{y}{h} \tag{2.4}$$

with
$$A_p = \frac{3\left(1-\nu^2\right)}{16}\left(1-\frac{b^4}{a^4}-4\frac{b^2}{a^2}\log\frac{a}{b}\right). \tag{2.5}$$

Reflecting the stiffness of the diaphragm, A_p is a function of the so called "solidity ratio of boss and diaphragm radii" (b/a). In (2.5), ν is Poisson's ratio and b is the boss radius. In these two equations, the effects of a finite diaphragm boss thickness and internal stress are not taken into account. Experiments do show that a bossed circular diaphragm displays good linearity[5].

2.2.3.2 Corrugated Circular Diaphragm

Corrugations introduced into a diaphragm alter the coefficients of the linear and cubic terms in Equation (2.1). The load-deflection relation of a corrugated diaphragm is given by[13]:

$$\frac{Pa^4}{Eh^4} = A_p\left[\frac{y}{h}\right] + B_p\left[\frac{y}{h}\right]^3 \tag{2.6}$$

with $A_p = \dfrac{2(q+2)(q+1)}{3\left(1-\left(\frac{\nu}{q}\right)^2\right)}$, and $B_p = \dfrac{32}{q^2-9}\left[\dfrac{1}{6} - \dfrac{3-\nu}{(q-\nu)(q+3)}\right]$

where q is the corrugation quality. For sinusoidal corrugation profiles, q is defined

as
$$q^2 = \frac{s}{l}\left(1+1.5\left(\frac{H}{h}\right)^2\right)$$

with H being the corrugation depth, s the corrugation arc length and l the corrugate spatial period. For a flat diaphragm, q=1.

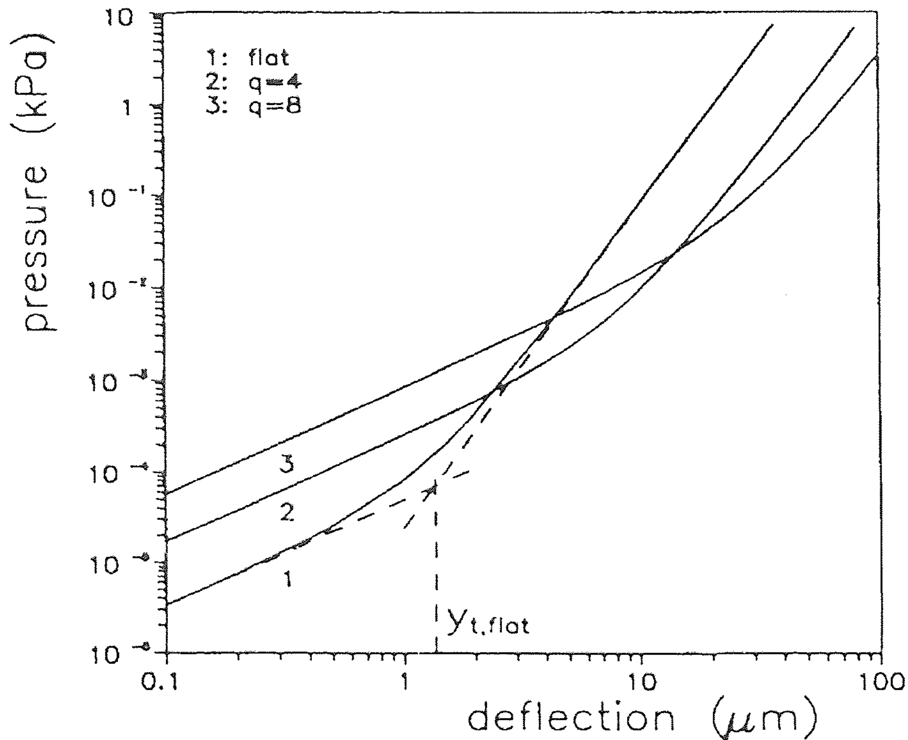

Figure 2.2 Load-deflection Characteristics of Flat and Corrugated Diaphragms[16]

Experimental studies of corrugated diaphragms show that in the small deflection region, the introduction of corrugations extends the linear portion of the load-deflection characteristics[16]. Figure 2.2 shows the comparison of three diaphragms all with diameter a=0.5mm, h=1μm and E=3Gpa (polyimide diaphragm).

2.2.3.3 Bossed and Corrugated Circular Diaphragm

If a center boss is introduced into the corrugated structure, modifications of the linear and non-linear coefficients are needed. Load-deflection relations can be expressed by adding two modify factors in Equation (2.6) to reflect the influence of the boss. For a small deflection, the load-deflection relation can be written as[20]

$$\frac{PR^4}{Eh^4} = A_p n_p \frac{y}{h} \tag{2.7}$$

where $$\frac{1}{n_p} = \left(1 - r^4\right)\left(1 - \frac{8qr^4\left(1 - r^{q-1}\right)\left(1 - r^{q-3}\right)}{(q-1)(q-3)\left(1 - r^{2q}\right)}\right)$$

and r is the ratio of boss radius to diaphragm radius. For large deflection, the influence of a boss on the cubic term should be considered. A modification factor similar in magnitude to n_p but of more complicated form, should be added to B_p.

Figure 2.3 shows the characteristics of two 3.5mm diameter, circular diaphragms with 80% center bosses, one being flat and the other corrugated[21]. The thickness of the diaphragms are about 1.2μm and the corrugation depth is 12μm. We can see that the diaphragm having corrugations has an apparently improved linearity.

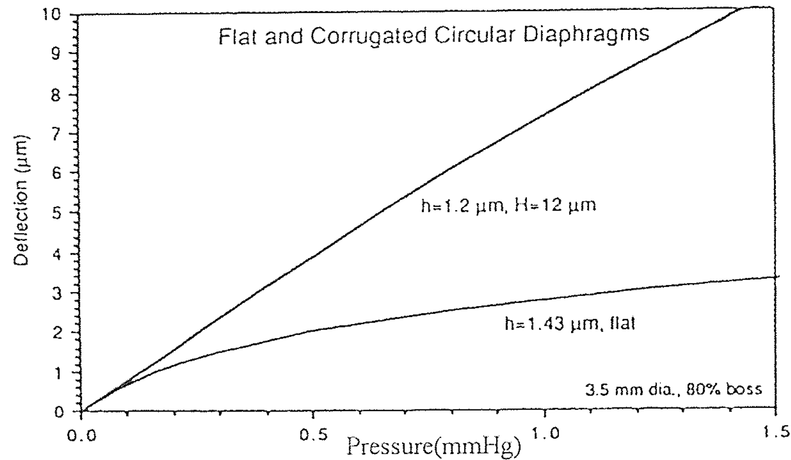

Figure 2.3 Comparison of Flat and Corrugated Diaphragm Response[21]

2.2.3.4 Non-Planar Square Diaphragm

For a bossed or corrugated square diaphragm, and a square diaphragm with both boss and corrugations, due to the complexity of geometry, no simple simulation models can be established. It is very difficult to obtain analytical expressions of load-deflection relations for these diaphragms. X. Ding has reported his studies of the behavior of square silicon diaphragms with a boss and corrugations[20], see Figure 2.4.

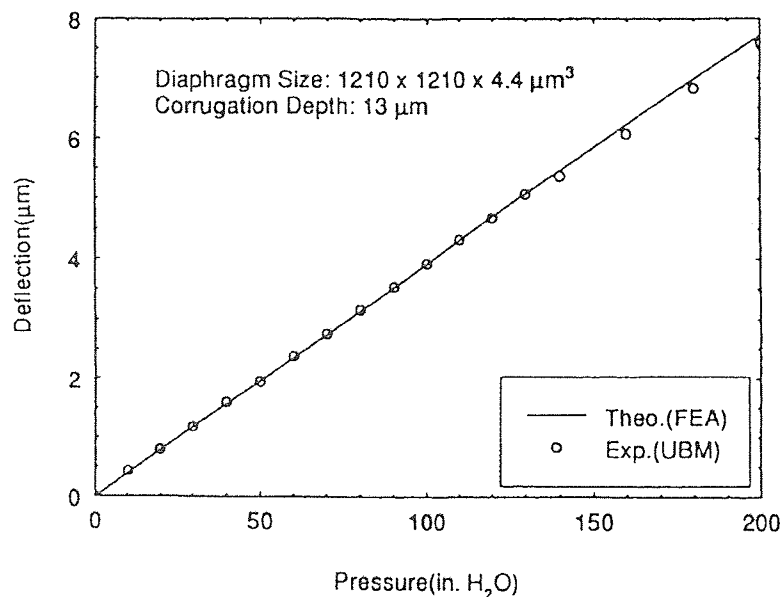

Figure 2.4 Measured and FEA(finite element analyses) Calculated Diaphragm Deflection versus Pressure for a Diaphragm with a Boss and Corrugations Used for Low-pressure Sensor.[20]

Y. Zhang, S. B. Crary, and K. D. Wise have reported a workstation-based simulation module-CAEMENS-D for micromachined silicon diaphragm structures, which can be used to simulate non-planar sensors[19]. Their research shows that the linearity in the midrange response is improved by using a bossed diaphragm and the overall response characteristics are smoothed. But the sensitivity in the low and middle pressure ranges is reduced. Some experimental results regarding the performance of non-planar square diaphragms are shown in Figure 2.5.

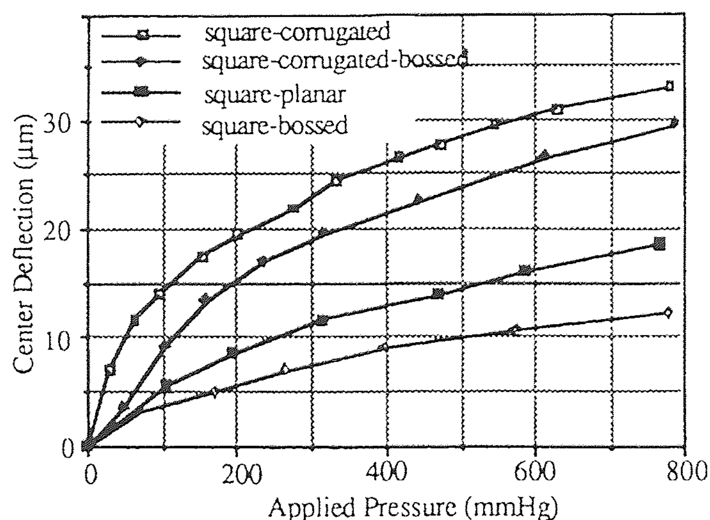

Figure 2.5 Deflection vs. Pressure for Various Square Diaphragm Structures [18]

Based on these studies, we can conclude that bossed and corrugated diaphragms have better response characteristics than the conventional planar diaphragms but at the expense of reduced sensitivity. By using appropriate deflection sensing techniques with the non-planar structures discussed above, it is possible to fabricate pressure sensors with higher sensitivity, larger dynamic range and better linearity than sensors with conventional planar diaphragms.

The sensor described in this paper employs a bossed structure. The boss works both as a linearity-enhancing method and as an ideal optical fiber support with the V-groove micromachined on it.

2.3 Principles of Modulation and Compensation

For a multimode optical fiber as shown in Figure 2.6, the luminous flux distribution formed by its output end is given by [24]

$$\Phi(r,z) = \frac{K_0 I_0}{\pi R^2} \cdot \exp\left[-r^2 / R^2(z)\right], \tag{2.8}$$

where I_0 is the intensity of the light source coupled into the fiber, K_0 represents the losses in the source fiber, and $\Phi(r,z)$ represents the luminous flux density at point (r,z). $R(z)$ is called effective radius of the output optical field, which is defined by

$$R(z) = a_0\left[1 + ktg\,\theta_0 (z / a_0)^{\frac{3}{2}}\right]. \tag{2.9}$$

Here, a_0 is the radius of the fiber core, θ_0 is the maximum incident angle of the fiber, and k is a constant depending on the coupling condition of the light source.

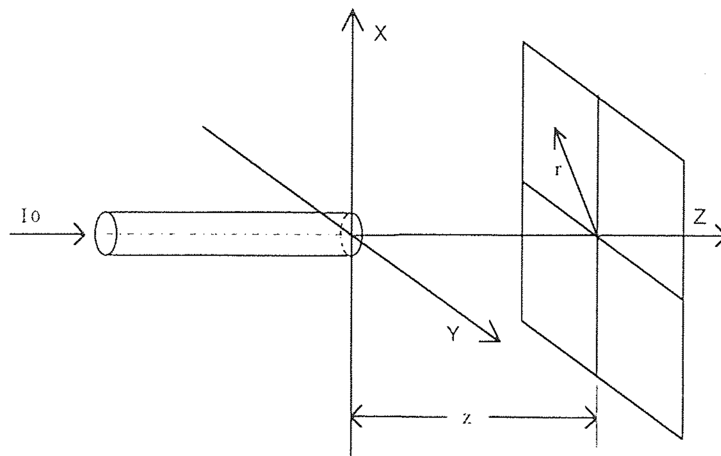

Figure 2.6 Multimode Optical Fiber in Radially Symmetric Coordinates

When a light detecting fiber is put in the output optical field formed by the source fiber, the light intensity output from a receiving fiber positioned at (r, z) is

$$I(r,z) = \iint_{S} \frac{K_0 K I_0 \exp(-\sum \eta_i r_i)}{\pi R^2(z)} \cdot \exp\left[-r^2 / R^2(z)\right] ds \tag{2.10}$$

where K represents the loss in the receiving fiber, $exp(-\sum \eta_i r_i)$ represents the additional losses in the receiving fiber caused by fiber bends[25], and s is the receiving fiber core area.

To avoid the integral in Equation (2.10), the intensity at the fiber center can be used approximately to denote the average light intensity on the end face of the receiving fiber. Thus, the output signal from a detecting fiber positioned at (r,z) can be written as:

$$I(r,z) = \frac{s K_0 K I_0 \exp(-\sum \eta_i r_i)}{\pi R^2(z)} \cdot \exp\left[-r^2 / R^2(z)\right]. \tag{2.11}$$

Based on this equation for the optical fiber system shown in Figure 1.4, an analytical modulating function can be derived by defining a coordinate system as shown in Figure 2.7.

The intensities coupled from the source fiber positioned at $(0,x)$ into the two receiving fibers as shown in Figure 2.6 can be expressed, respectively, as

$$I_1(r,z) = \frac{s_1 K_0 K_1 I_0 \exp\left[-\sum \eta_i r_i\right]}{\pi R^2(z)} \cdot \exp\left[-\frac{(x-a)^2}{R^2(z)}\right] \tag{2.12}$$

and

$$I_2(r,z) = \frac{s_2 K_0 K_2 I_0 \exp\left[-\sum \eta_i r_i\right]}{\pi R^2(z)} \cdot \exp\left[-\frac{(x+a)^2}{R^2(z)}\right], \tag{2.13}$$

where x is the displacement of source fiber from z-axis, a is the radius of the fiber. From above equations the ratio of output intensities is

$$I1/_{I_2} = \frac{s_1 K_0 K_1 I_0 \exp_1\left(-\sum \eta_i r_i\right)}{s_2 K_0 K_2 I_0 \exp_2\left(-\sum \eta_i r_i\right)} \cdot \exp\left[\frac{4ax}{R^2(z)}\right]. \tag{2.14}$$

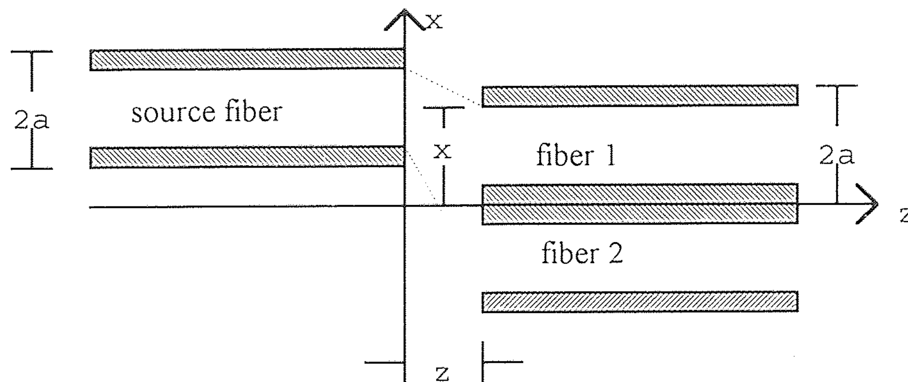

Figure 2.7 Light Source Fiber and Receiving Fibers in Rectangular Coordinates

If the two receiving fibers are the same kind and are taken from the same optical fiber cable, the two receiving fibers can be considered identical. Then, the losses and the receiving core areas of the two fibers can be canceled in Equation (2.14). For small displacement of the source fiber, the logarithm of the light intensities ratio of the two receiving fiber can be expressed as

$$Ln\left(\frac{I_1}{I_2}\right) = \frac{4ax}{a_0^2\left[1 + ktg\theta_0\left(\frac{z}{a_0}\right)^{3/2}\right]^2}. \tag{2.15}$$

It shows that the logarithm of the intensity ratio has a linear relation with the displacement of the source fiber, and furthermore, it is independent of the light source intensity I_0, independent of the losses in the fibers, and independent of the losses caused by fiber bends. These are the great advantages of this simple sensing mechanism.

CHAPTER 3

FABRICATION

1.1 Introduction of Silicon Micromachining

Silicon is being increasingly employed in a variety of miniature sensors and actuators. In these devices silicon plays multidiciplinary roles. Besides its conventional usage as an ideal semiconductor, it is silicon's excellent mechanical properties that is emphasized in these devices. Micromechanical structures of silicon in the forms of diaphragms, cantilevers and beams are the most important components of these miniature devices. For the fabrication of these silicon based microsystems, silicon michromachining is a key technology.

Etching is the main method of silicon micromachining. There are several different types of etching. They are classified as wet chemical etch, plasma etch(PE), reactive ion etch(RIE) and dual PE and RIE. According to the properties of silicon and other materials, by using appropriate enchant or etching method, the required microstructures can be attained starting from a standard silicon wafer. For the fabrication of the silicon optical fiber pressure sensor discussed here, a typical fabrication process is required. The process sequence is shown in Figure 3.1.

Step 1: Formation of etching mask. Approximately 1 μm SiO_2 is produced by high-temperature oxidation. It will be used as mask for KOH etching. For other enchants or etching methods, different materials may be used as etching mask, and the thickness and the formation method of the mask layer may be different.

Step 2—4: Photolithography. Patterns are transferred to the etching mask.

Step 5: Mask Etching. Without protection of photoresist, patterned SiO_2 is etched off by buffered hydrofluoric acid (HF).

Step 6: KOH deep etching. After striping off the remaining photoresist, the wafer is dipped in KOH water solution for etching of the substrate. The etch depth is determined

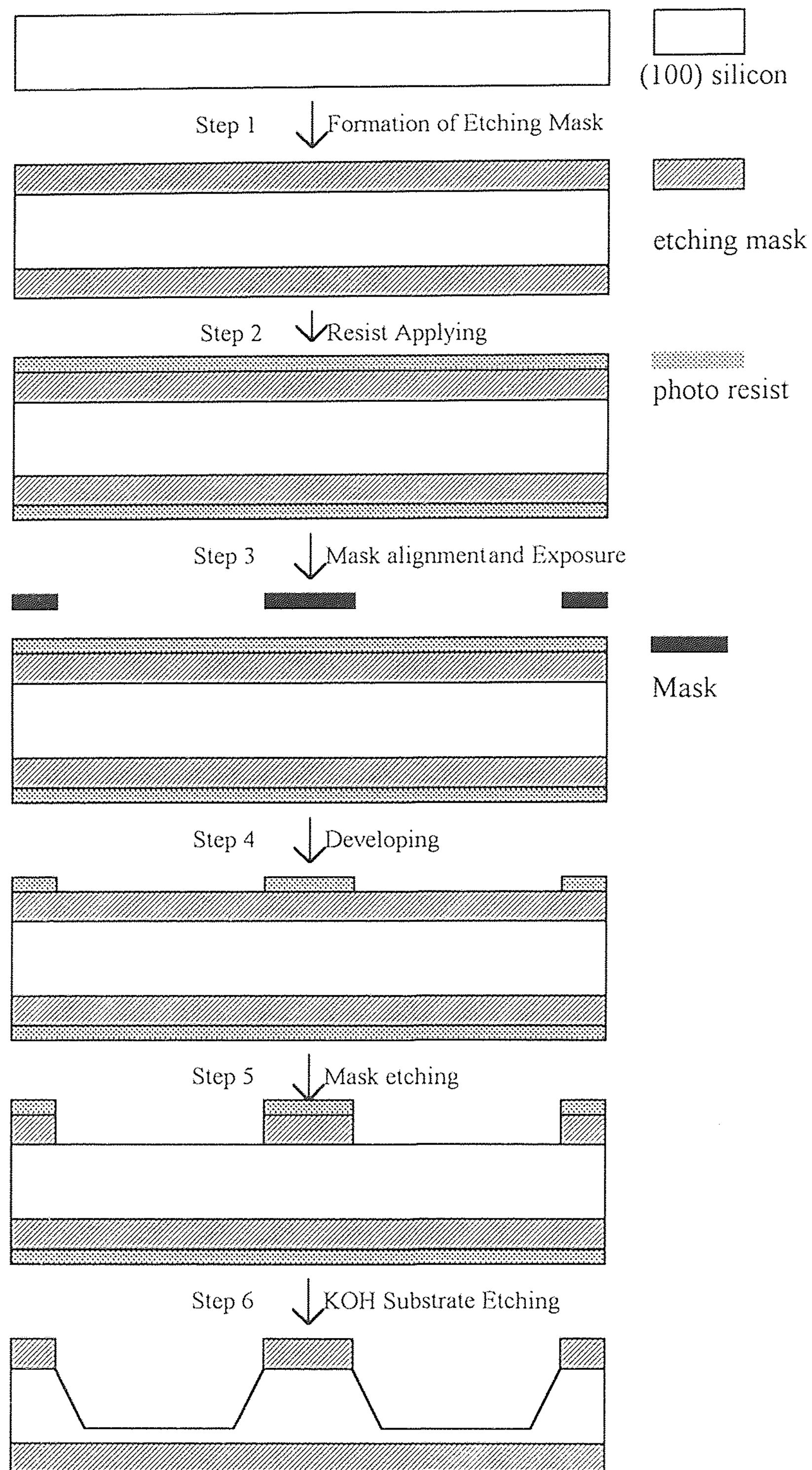

Figure 3.1 Fabrication Process Sequence for Pressure Sensing Silicon Diaphragm

by etching time, KOH concentration and temperature.

For a more complex silicon microstructure some steps of the process will be repeated one or several times and some other steps may be involved.

Details of mask making and etching process of the silicon pressure sensor are described in the following sections.

3.2 Mask Design and Making

To get a sensor structured as Figure 2.1, two photo masks are needed. The second mask is needed only for the formation of the over pressure protection. To lower the cost and simplify the fabrication process, one mask is enough to get the fundamental structure of the sensor without sacrificing the characteristics of the sensor.

Figures used as mask are shown in Figure 3.2.

In Figure 3.2, (a) is to be used to get the top cover of the sensor; (b) is to be used for creating V-grooves which are symmetric to the grooves in the die with a sensing diaphragm.(to obtain the function of over-pressure protection, another mask is needed); (c) is used for the silcon support and (d) is used for the silicon die with bossed diaphragm and V-grooves.

The unit for the dimensions shown in Figure 3.2 is μm.

Figure 3.3 shows the side views of fibers in V-grooves.

Due to the anisotropic property of silicon, a V-groove can be gotten by etching the (100) oriented silicon wafer[25].When a V-groove is formed, the etching will be almost stopped. Detailed discussion is given in Section 3.4.

The dimensions of the V-grooves depend on the window width on the mask layer and the etch rate ratio of differently oriented plane of crystalline silicon. The dimensions of V-grooves should be designed to fit optical fibers exactly as shown in Figure 3.3.

A nonstandard method is used to make the mask.

First, the precise figures shown in Figure 3.3 are created by using Mentor Graphic

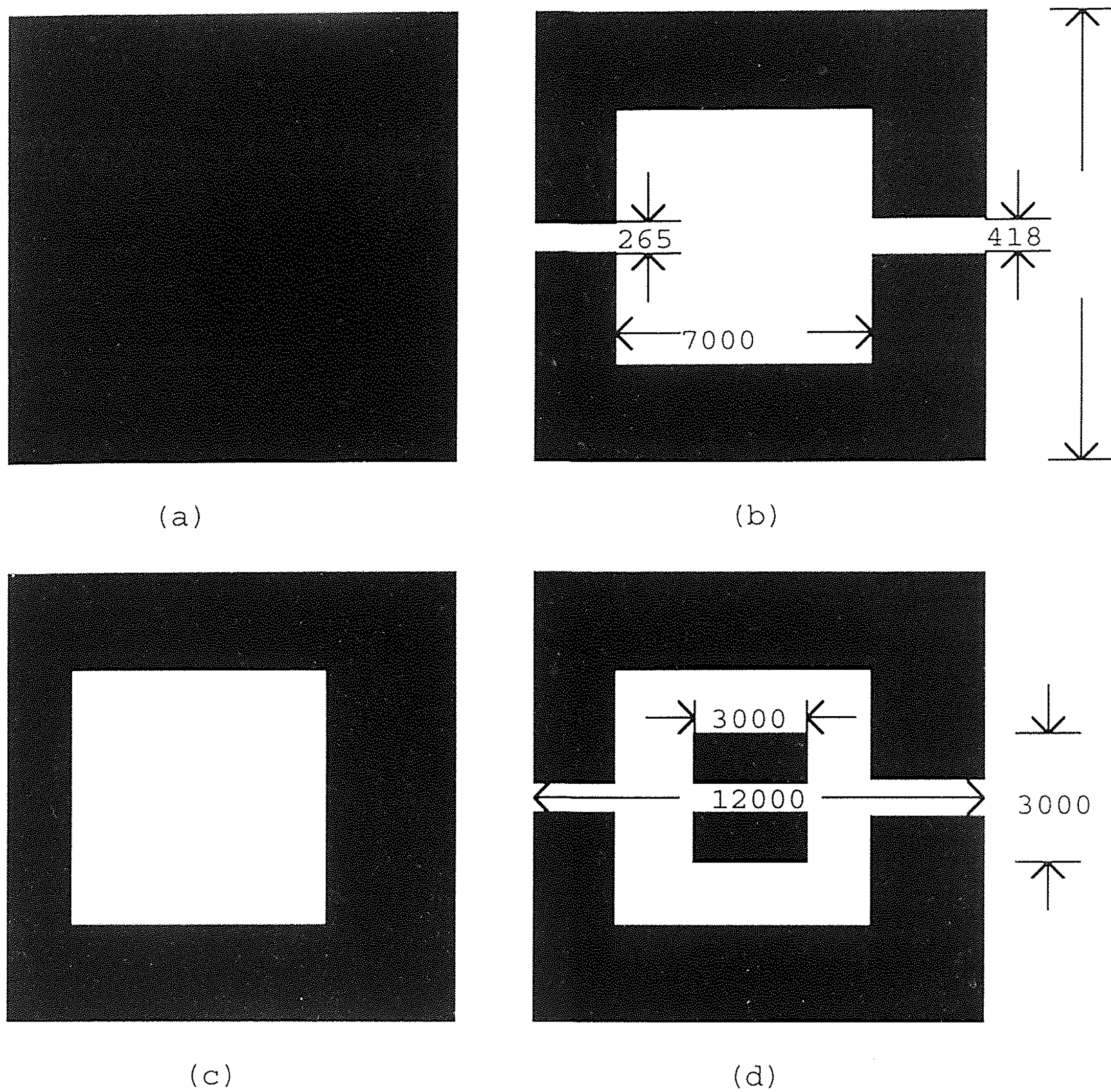

Figure 3.2 Figures for Mask Design (Dimensions are in μm)

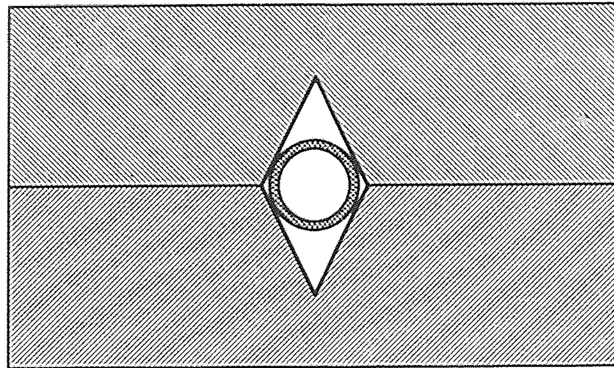

(a) Left side

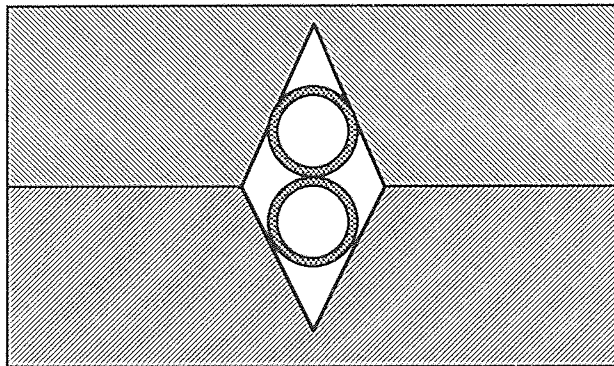

(b) Right side

Figure 3.3 Optical Fibers in V-grooves

IC station software and are printed out with enlargement.

Secondly, the printout figures are arranged and posted on a flat board. Using a SLR camera with a zoom lens, the figures are exposed on 35mm film. Since the dimension of 35mm film is standard and known, the figures can be roughly reduced to required sizes by adjusting the position and the focus length of the camera according to the position of the figure in the view finder of the camera. See Figure 3.4.

The developed film is used directly as a mask. For more precise dimensions or for smaller structures, standard mask making methods should be used.

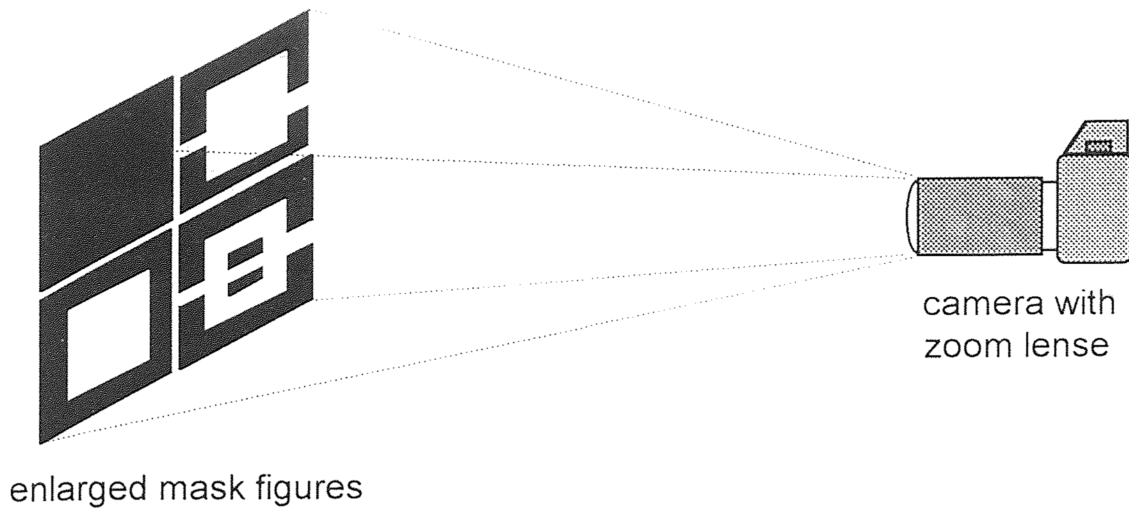

Figure 3.4 Mask Created by SLR Camera

3.3 Wafer Processing

3.3.1. Wafer Cleaning and Oxidation

5" 5Ω-cm n-type (100) oriented single side polished silicon wafers are used. To get a better etching surface, double side polished silicon wafers are preferred.

The wafer is processed in a cleanroom according to the procedures below:

- scribe identification
- P-clean, 5:1 H_2SO_4:H_2O, 110 ^{0}C, 10 minutes
- Rinse in HOT DI water, 10 minutes
- Rinse in COLD DI water, 5 minutes
- Spin Dry
- Furnace pre-clean, 100:1 H_2O:HF, 1 minute
- Rinse in COLD DI water, 10 minutes
- Spin dry
- Steam oxidation

3.3.2 Photolithography

- Photoresist application. Spin time: 20 second; Spin speed of vacuum spindle: 3000 rpm. Photoresist: Micro Posit® Resist S1400-30.
- Pre-exposure baking. Temperature: 80°C; Baking time: 20 minutes.
- Exposing. System: Model-800 Wafer to Mask Alignment and Exposure System, manufactured by Applied Materials Cobilt Division. Exposing time: 35 Seconds.
- Developing. Developer : Micro Posit®Developer MF®-320.
- Post baking. Temperature: 120°C; Baking time: 20 minutes.

3.3.3 Oxide Etch

After photolithography, the wafer is put in buffered hydrofluoric acid (HF), which etches SiO_2 fast but without attacking the photoresist and SiO_2 under the photoresist which is going to be used as etching mask.

3.4 Anisotropic Etching of Crystalline Silicon

3.4.1 Introduction

Some aqueous alkaline solutions dissolve a given crystal plane of silicon or other semiconductors much faster than other planes. This is known as anisotropic etching and has been studied for a long time [27]. The reason of the orientation-dependence is that in lattices, the arrangement of atoms on some planes are different from the others. For a plane which is more closely packed than the other planes, more energy is needed to dissolve the atoms on such a plane, so that the etch rate of the plane is slower than the rate of other planes. But the etch rate ratio for different planes depends on not only the atom arrangements, but also the properties of etchants and the temperature.

The anisotropic etching of silicon has been used for creating a variety of silicon structures in a highly controllable and reproducible manner. Typical structures created by anisotropic etching include thin planar diaphragms, corrugated diaphragm, bossed

diaphragms, V-grooves, beams, and cantilevers. These structures have been used for fabrication of passive mechanical elements, sensors and actuators, and micro-optical components.

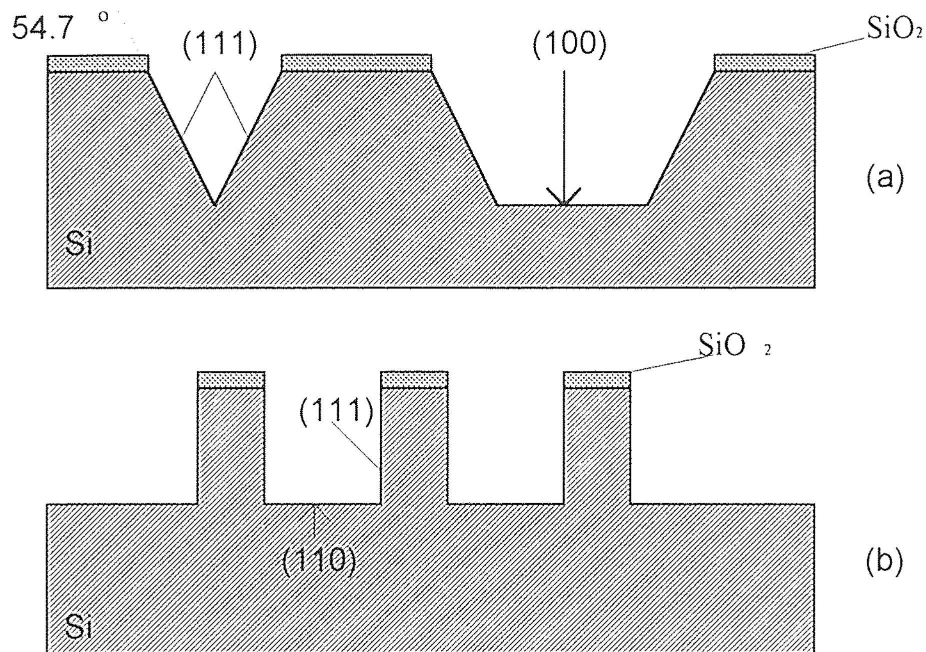

Figure 3.5 Orientation Dependent Etching
(a) Through window patterns on <100>-oriented silicon
(b) Through window patters on <110>-oriented silicon [25]

Figure 3.5 shows a typical structure created by orientation-dependent etching of crystalline silicon. In Figure 3.5a, The V-shaped groove in <100>-oriented silicon wafer is formed by opening a window in the silicon oxide mask and etching long enough. If the window is sufficiently large and etch time is short , a U-shaped groove will be obtained, as shown in the right of the figure. The edges of the two grooves are (111)-planes at an angle of 54.7° from the (100)-surface. If etching begins from a <110>-oriented silicon wafer, straight-walled grooves with sides of (111)-planes will be obtained, as shown in Figure 3.5b.

3.4.2 Etchants for Anisotropic Etching of Silicon

The important properties of anisotropic etchants of silicon are anisotropy, selectivity, handling, and IC process compatibility. All silicon anisotropic etchants are aqueous alkaline solutions. They can be classified as organic etchants and inorganic. Solutions consisting of ethylenediamine, water, and pyrocatechol(EDP) are the most widely used organic etchants. Aqueous solutions of KOH are the most popular inorganic etchants. From both kind etchants, a smooth surface can be obtained with fast etching rate and satisfying selectivity of different orientations. But they also have their own disadvantages. EDP is highly toxic and thus requiring special facilities for handling. KOH is less toxic and easy for handling, but having a fast etching rate for SiO_2. For deep etch of silicon, a thick thermal oxidation layer is required.

3.4.3 Etching Process

In the fabrication process of the silicon pressure sensor discussed here, KOH and water solution is used for its adequate etch rate and ease of handling.

Ammonium hydroxide-water (AHW) solutions are also tried for its low etching rate of SiO_2. But experiments show it could not be used as substitutes for KOH. Etching rate for silicon is too slow, and a coarse etching front is observed.

To create a silicon diaphragm with required thickness, the etch rate and etch time should be controlled. For aqueous KOH solutions with concentration in the range of 10-60%, an empirical formula can be used for calculation of the silicon etch rate[27]:

$$R = k_0 [H_2O]^4 [KOH]^{1/4} e^{-E_a/kT} \qquad (3.1)$$

Square brackets [ ] denote "concentration".

For a <100>-orientation, E_a= 0.595eV and k_0=2480 μm/h•(mol/liter)$^{-4.25}$; for <110>-orientation, E_a= 0.60eV and k_0=4500 μm/h•(mol/liter)$^{-4.25}$.

According to calculated results from (3.1), and by experiments, a 10% concentration KOH solution is chosen. The temperature is controlled at 60°C. Although the concentration and temperature are not at the optimum values for silicon anisotropic etching, considering the thickness of SiO_2 is about 0.5μm, this is an appropriate combination.

The finished wafer is expected to be as Figure 3.6. But in the fabrication process, apparent corner recessing effect is observed. To obtain silicon structures close to Figure 3.6, compensations of corners should be considered in mask design. A modified mask design is shown is Figure 3.7.

3.4 Assembly and Packaging

The finished wafers, including a die, a support and a silicon frame with V-grooves, and the optical fibers are bonded by epoxy glue. Then the bonded structure is glued on a metal support which has a pressure inlet and a protection shell.

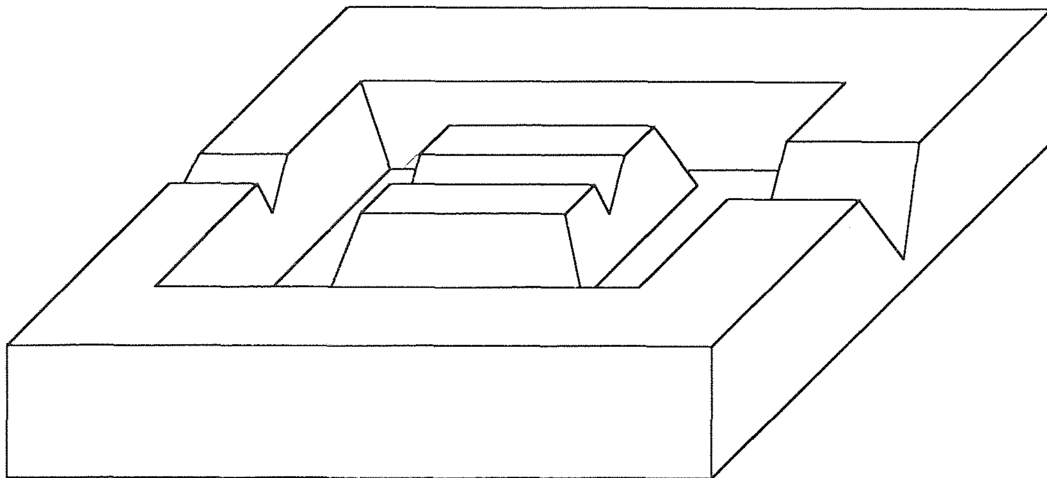

Figure 3.6 Finished Wafer

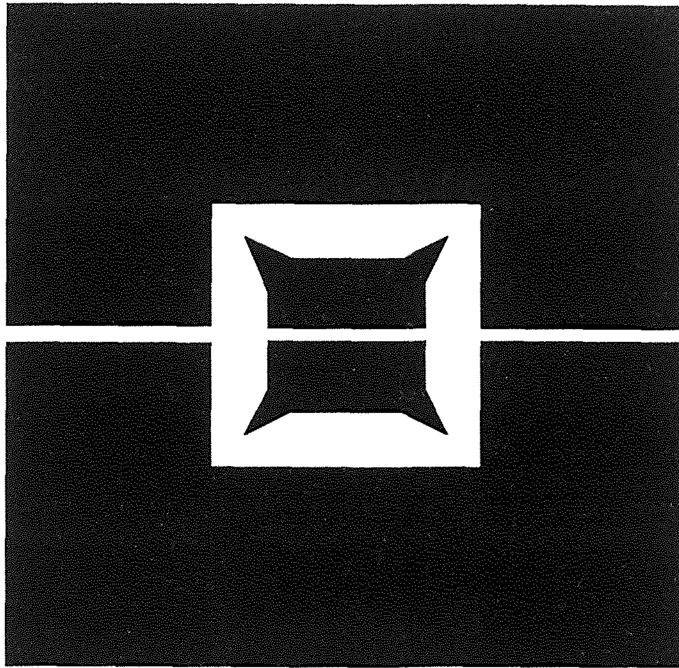

Figure 3.7 Modified Mask Design

CHAPTER 4

SIGNAL PROCESSING

4.1 An Overview of the Sensor

The working system of the silicon optical fiber pressure sensor is schematically shown in Figure 4.1. It consists a light source, the sensor element, an input optical fiber, two output optical fibers, two detectors and a signal processing part. Except that it has one extra output fiber and one extra detector, its structure is almost the same as any other typical optical fiber sensor system.

Unlike an optical fiber communication system, which is very selective about the light sources and detectors, various light sources and detectors have been used in different optical fiber sensors. In general, the determinant factors about the selections of light sources, detectors and fibers used in a sensor are often the modulation method and economy consideration. For modulation of phase and polarization, single mode fibers and coherent light sources are required, such as lasers, semiconductor laser diodes; for modulation of intensity or spectral distribution, multimode fibers and non coherent light source can be used.

For signal processing, there are two basic ways. One is using a dedicated circuit for signal processing. The main tasks of the circuit is signal pre-amplification and logarithm operation. The advantage is low cost and compact size. The other one is using the computer for signal processing. The advantage is high precision, ease of signal calibration and handling. Furthermore, if one uses a computer, it is very convenient to store data for future applications.

Another possibility is the combination of these two ways. Using a microprocessor with necessary circuits, it is possible to get a high precision sensor which has digital ready output and can be easily used for automatic control.

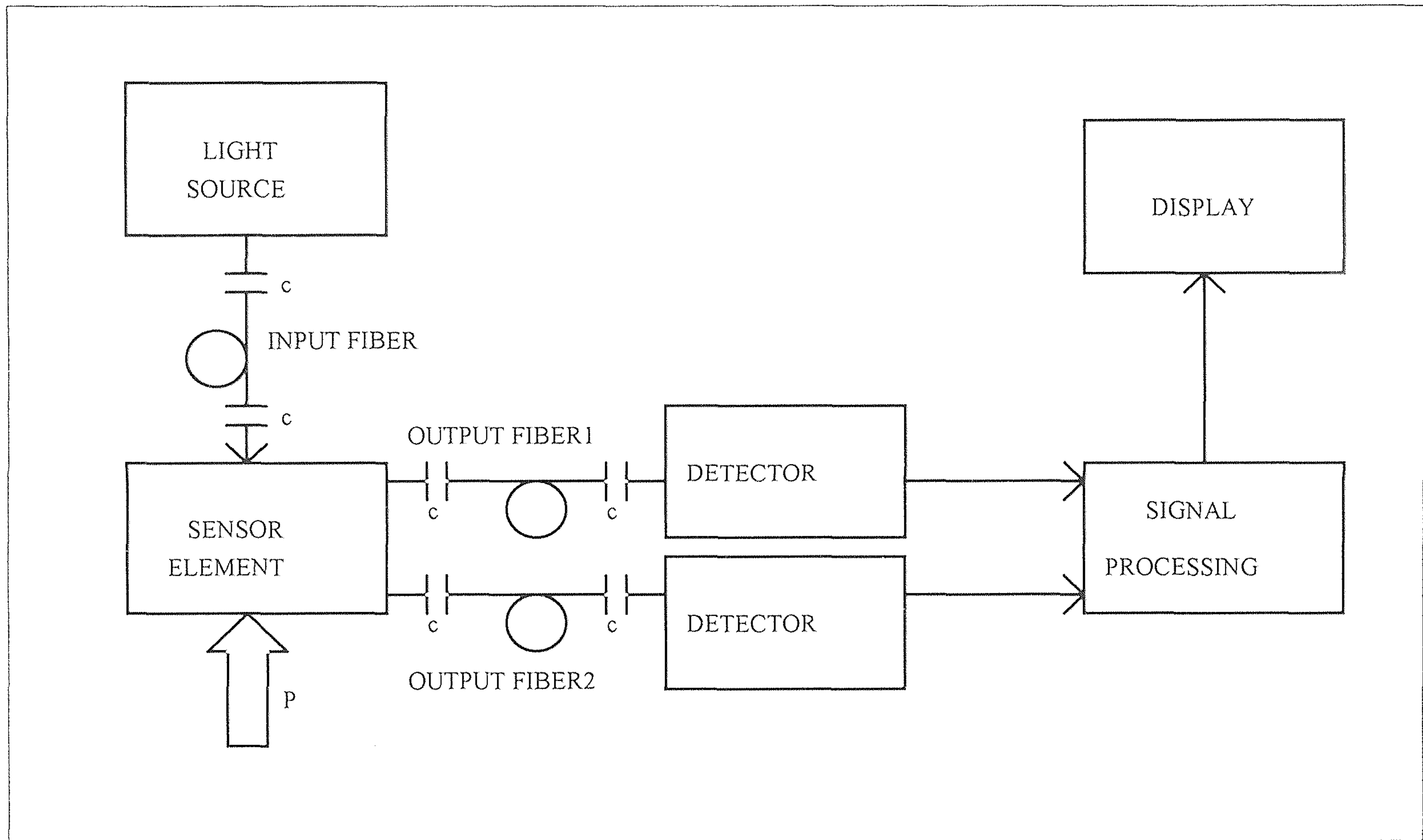

Figure 4.1 Block Diagram of the Silicon Optical Fiber Pressure Sensor
(C: connector, P: pressure)

4.2 Light Source

Since the sensor discussed in this thesis is an intensity modulation type, almost all types of light sources can be used: incandescent lamps(tungsten lamp), gas lasers(He-Ne lasers), light emitting diodes(LED), and semiconductor laser diodes.

In our tests of the sensor, a tungsten light and He-Ne laser are used and the results are compared.

4.3 Light Detecting

Light detecting is one of most important processes of a optical sensing system. In this process, a light signal is converted to an electrical signal for further processing. High sensitivity, fast response and linearity are the fundamental requirements for light detecting devices.

For the sensor discussed here, the most important property of detectors we are concerned with is its linearity. And we hope we can get two identical detectors.

For their compactness and ease of use, semiconductor photo detectors are the most often used detecting devices in optical fiber sensors. There are currently four principal types of semiconductor photo detectors: the PIN-diode, the avalanche photo diode(APD), the PIN-FET hybrid module, and photo conductors.

Silicon photo diodes are the most common detectors used in instrumentation. The spectral response covers the visible and near infrared. The linearity and dynamic range is excellent and obtaining a signal is simple. In the testing experiments of the sensor, two silicon photo diodes(SD1420-002) provided by Micro Switch are used.

4.4 Signal Amplification and Processing

The method of signal processing is schematically shown in Figure 4.2. The photo currents from two photo diodes are pre-amplified first and then input into two logarithmic amplifiers. The difference of the logarithm is obtained from the output of a voltage

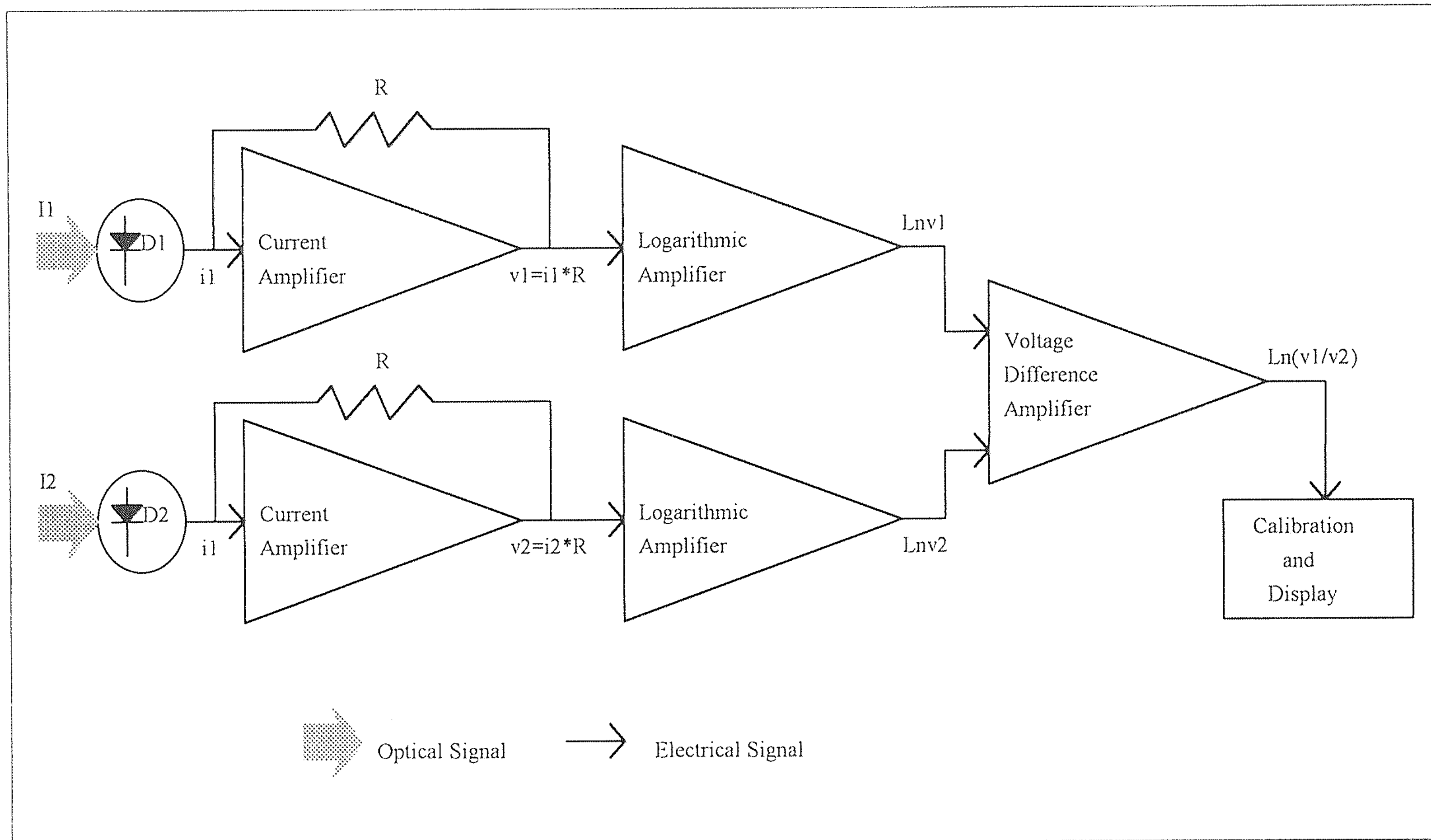

Figure 4.2 Block Diagram of Signal Amplification and Processing

difference amplifier. This signal is proportional to the logarithms of the ratio of light inputs of the two photo diodes. The circuit to fulfill the above function is shown in Appendix A.

In the testing experiments of the sensor described here, a computer connected to two digital multimeters by IEEE-488 interface is used for signal processing. A detailed description is given in Chapter 5.

CHAPTER 5

EXPERIMENTS

5.1 Experimental Set-Up

A series of experiments have been performed to test the sensor. The basic experimental set-up for testing is schematically shown in Figure 5.1.

A He-Ne laser or tungsten lamp is used as light source. The light from the source is focused to the input end of a multimode optical fiber. The optical signal is modulated by the inlet pressure which is varied by changing the height of a water column in a vertically mounted glass tube. The modulated signals are received by other two multimode optical fibers and conducted to two silicon photo diodes. Then the received optical signals are

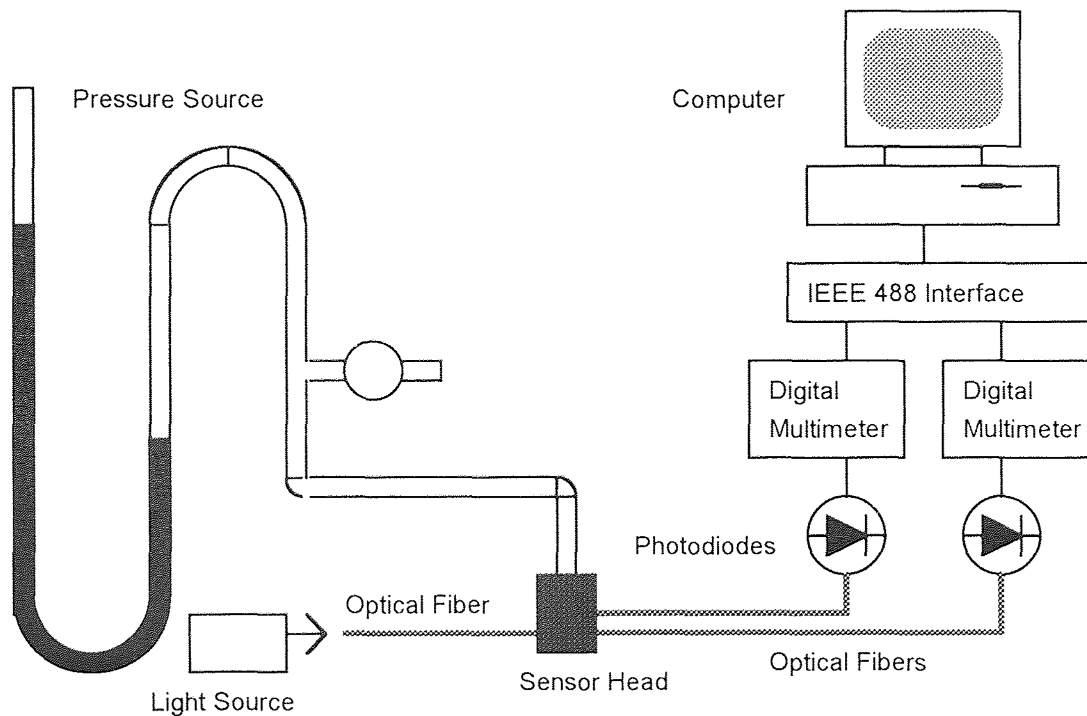

Figure 5.1 Schematic Depiction of the Experimental Set-Up for the Testing of Sensor

converted to two voltage signals by the photo diodes and transmitted to two digital voltmeter (Keithley 195A Digital Multimeter). Through the IEEE-488 interfaces between a computer and digital voltmeters, the signals are transmitted to a computer.

A computer program used for data acquisition and calculation is shown in Appendix B. By expanding the program, the computer's function in the system can be extended for signal processing, data analysis, data storage and transmission.

To obtain more precise quantitative measurements, a mechanical chopper and a lock-in-amplifier should be used. The chopper modulates the input light beam at a fixed frequency and at the same time provides the lock-in-amplifier the same frequency as reference. The outputs from the photo diodes are fed into the lock-in-amplifier, and the output of the amplifier can be input to the computer for calculation and further processing.

5.2 Measurement of Characteristics of Sensor

5.2.1 Measurement of Deflection and Response Characteristics

It is necessary and more convenient to perform several experiments before the bonding of optical fibers to the silicon diaphragm and even before the design of the silicon sensor. The linear response range can be obtained from experiments of the optical fiber system discussed in Chapter 2. And then, based on the load-deflection relation of the silicon diaphragm, we can decide the dimensions, thickness and the pressure range of a silicon diaphragm in our design.

Figure 5.2 shows the relation of deflection versus sensor output from experiments. The deflection is simulated by moving the output end of source fiber with a micro manipulator. The light source is a tungsten lamp. Multimode optical fibers with core diameter 200μm and cladding diameter 220μm are used as source fiber and receiving fibers. The distance between the output end of the source fiber and the input end of the receiving fibers is approximately 250μm. The experimental results agree with the theory we discussed in Chapter 2. For the range of total 300μm in two directions, the output

readings change linearly with the transversal displacement of source fiber or the deflection of a silicon diaphragm. Non-linearity occurs only at very large deflections for a silicon diaphragm deflections. Most silicon diaphragm's deflection will not exceed this linear region.

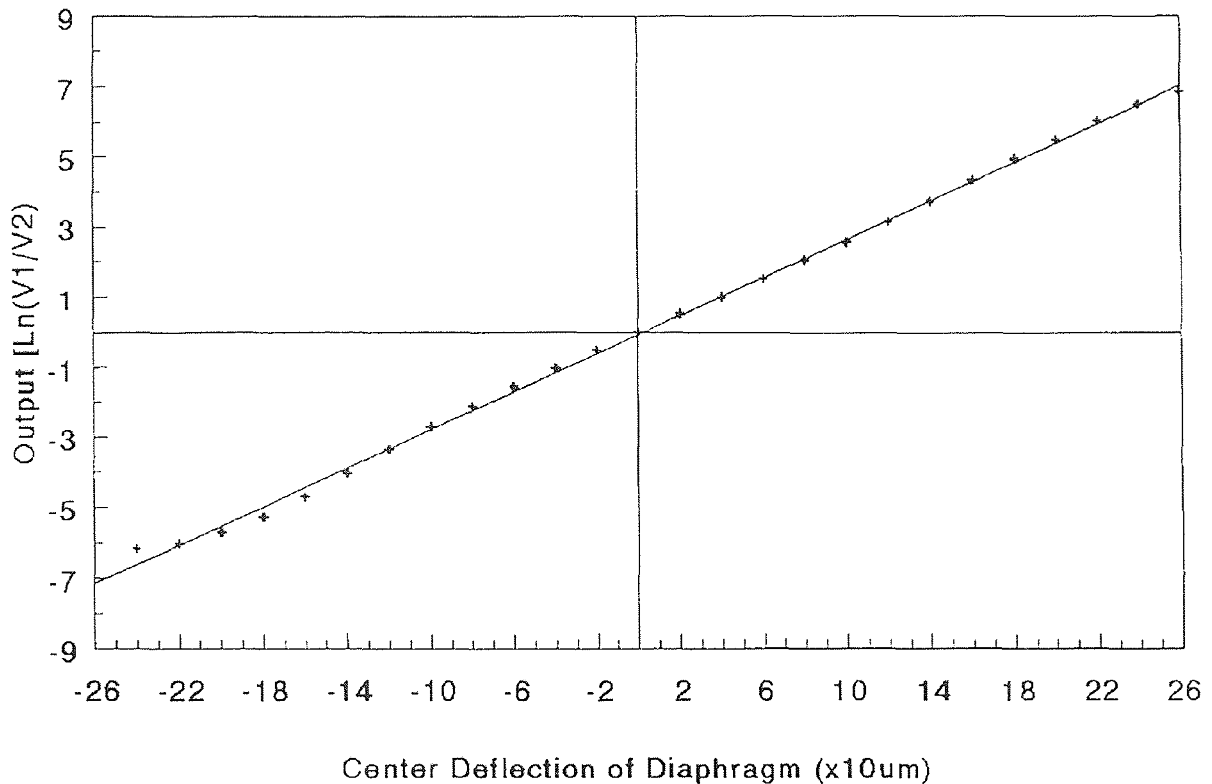

Figure 5.2 Output Signal vs. Diaphragm Deflection

The plot shows a little bit asymmetry. This is due to the fact that we set a position as zero point when the output reading is zero. Because of the asymmetry of the two detectors, the zero reading may occur when the source fiber is not in the center position of the two receiving fibers. Another possible reason is the cutting defects of the fiber ends. In general, since the linearity is unchanged no matter which point we choose as zero, a little asymmetry of the response will not affect the sensitivity and the precision of the sensor. But to optimize the sensor's working range, the alignment of the three fibers is important.

Light detectors and amplification should be chosen to be as closely matched as possible, if they could not be made identical; and the fiber end should be processed without defect to ensure good characteristics of the sensor.

5.2.2 Comparison of Different Light Source

Figure 5.3 shows the output signal versus the deflection of two different light sources, tungsten lamp and 6328Å He-Ne laser. Light intensities from the output end of the source fiber are kept unchanged. Other parameters such as fiber end distance and coupling condition of fiber to detectors are also unchanged.

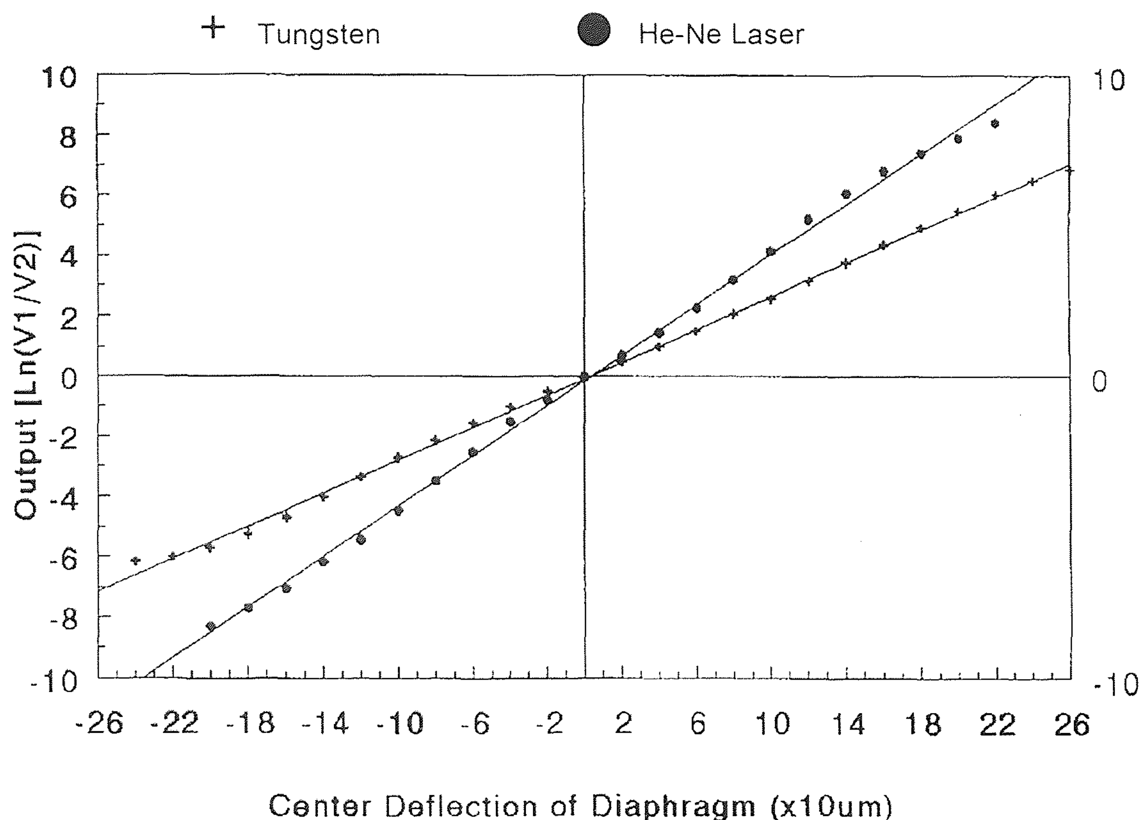

Figure 5.3 Comparison of Sensor's Characteristics for Different Light Sources

It is apparent that the response corresponding to white light from a tungsten lamp has better linearity than He-Ne laser and the dynamic range is wider than that for the laser. But the laser source gives a higher sensitivity. For the same deflection, using a laser a larger output signal will be obtained.

The difference of sensitivity and linear range comes from the coherent and non-coherent properties of the light sources. For non-coherent white light, the distribution is more stable and relatively flat. For coherent laser, the light distribution is concentrated in a smaller spatial range for the same light intensity. This means the gradient of intensity is larger, so that the ratio of light received by two receiving fiber is greater than the ratio for white light source and thus the output will be greater for the same deflection. Also for the relatively sharper distribution, the light detectable region is narrowed. This is why the laser source has a higher sensitivity but a narrower linear region.

5.2.3 Characteristics of Light Intensity Compensation

With two detecting fibers, without any other elaborate compensation method, the output of the sensor shows almost no variations for the fluctuations of light source intensity. For the same He-Ne laser but with intensity coupled into the source fiber being changed as much as 50%, plots of the output signal vs. deflection or the lateral displacement are shown in Figure 5.4. The two sets of data are very consistent with one another. This agrees with the theoretical analysis in Chapter 2.

5.2.4 Effect of End Distance Between Source Fiber and Receiving Fibers

To determine the effect of the distance between the source fiber and the two receiving fibers, experiments have been made using the same laser source and same parameters except the end distance z is changed 200μm (from about z=50μm to z= 250μm). Results are shown in Figure 5.5. Similar to the earlier comparison of laser source to white source, a small distance results in a large slope of the curve, i.e. high sensitivity; a large distance,

on the other hand, results in less sensitivity but with a little expansion of the linear range.

In fact, by defining the sensor's sensitivity as

$$S = \frac{d}{dx}\left[Ln\left({}^{I_1}\!/_{I_2} \right) \right] = \frac{4a}{a_0^2\left[1 + ktg\theta_0 \left({}^{z}\!/_{a_0} \right)^{3/2} \right]^2} \tag{5.1}$$

We can see that the sensitivity depends on the end distance z and source fiber's diameter.

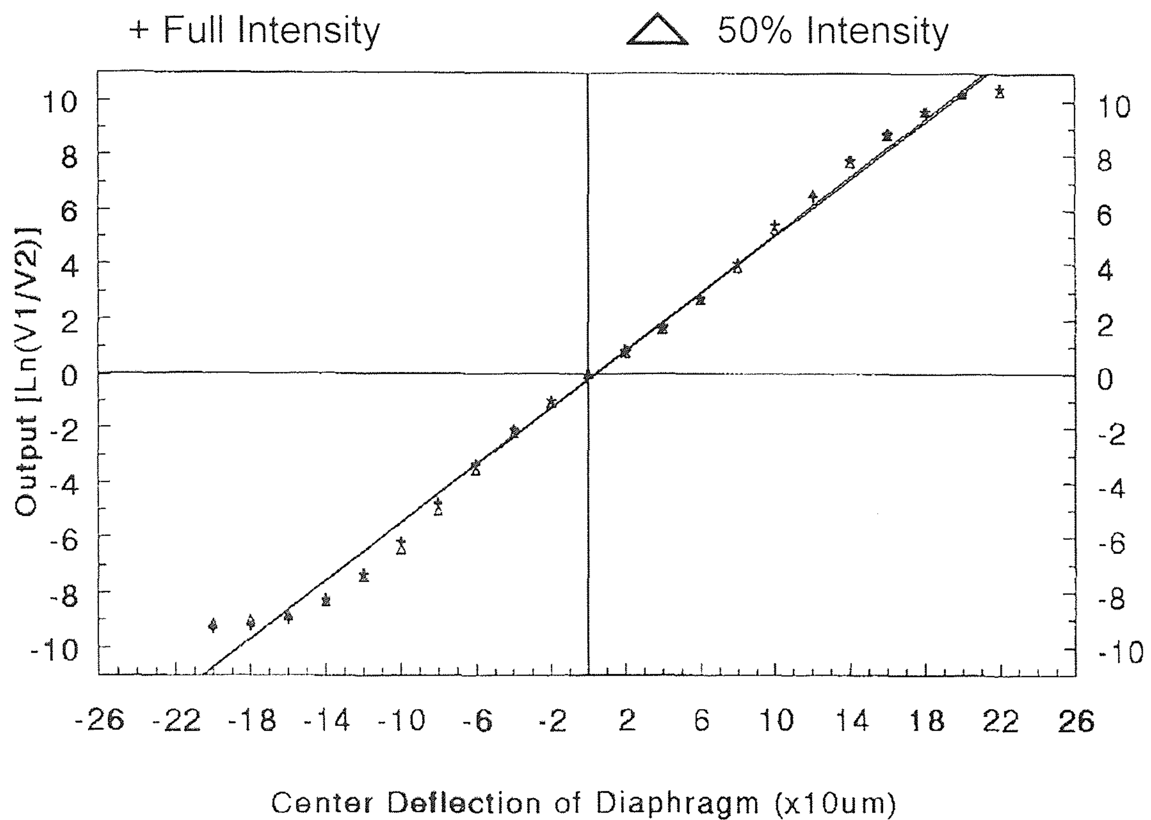

Figure 5.4. Characteristics of Light Intensity Compensation

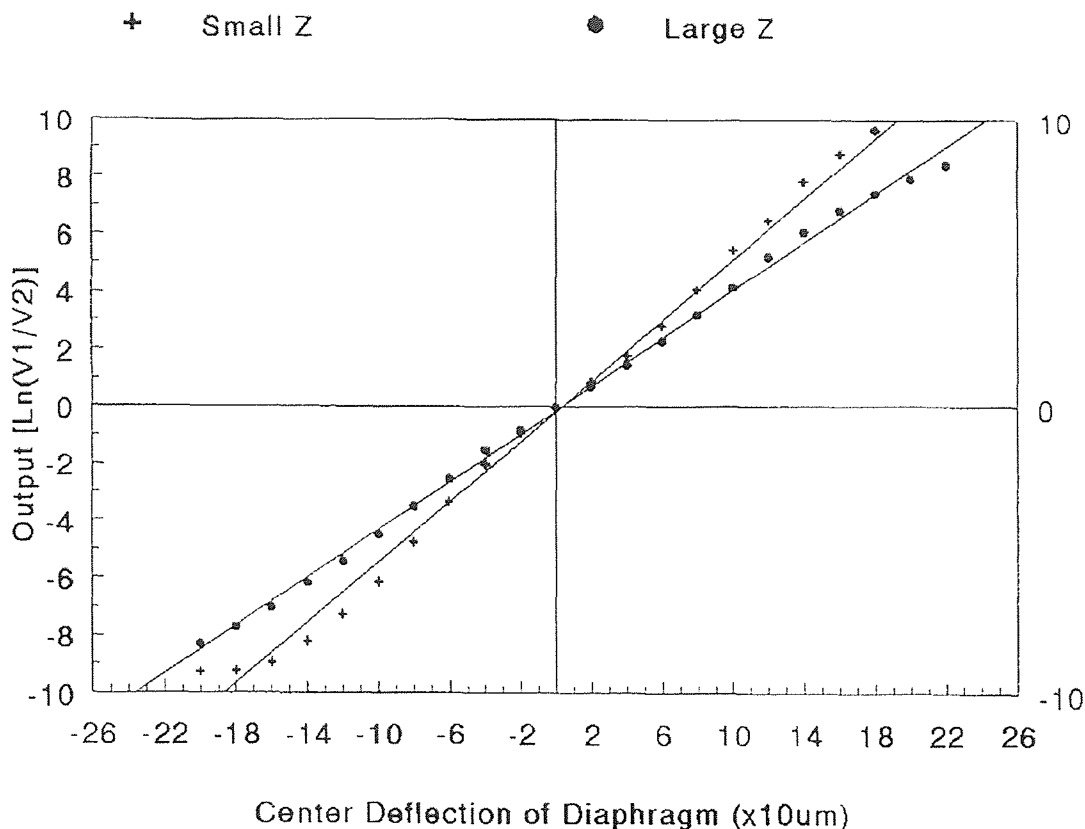

Figure 5.5 Response Comparison of Different Distances between Ends of Source Fiber and Receiving Fibers.

5.3 Discussion of Non-linearity and Application Limitations

From all experimental curves discussed above, a common feature is observed. All the curves have similar non linear tails, the tails curve to the same direction, no matter what kind of light sources are used, what is the end distance and what is the light source intensity. This disagreement with the conclusion we made in Chapter 2 comes from the approximation we made in the calculation of light intensity received by the testing fiber and possibly comes from the approximation of the fiber end light distribution described by Equation (2.8).

In the calculation of received light intensity of a receiving fiber, the center intensity is used to represent the average intensity over the fiber receiving end, for a linear light intensity distribution, this is not an approximation, it exactly equals the average intensity. For a non linear distribution, this may sometimes cause serious error. For example, when a

fiber is facing the source fiber, based on Equation (2.8), the light intensity at the center of the receiving fiber is far greater than the average intensity. At the same time, the calculation of the received light of the other fiber also has some error. The value of $Ln\left(I_1/I_2\right)$ may be higher than the real value at some position and be lower at some other position. But since the error is much less than the difference of light intensities received by two receiving fibers, it will not change the overall linear characteristics.

Another possible error source is the non linearity of the detectors. But since the same phenomenon appears for both small light intensity and large light intensity (Figure 5.4) without changing, this should not be the reason of the tails.

Since the non-linearity is apparent only at large deflection, this will not cause much trouble for sensor application. For most micro silicon sensors, the diaphragm deflection is much less than the diameters of a fiber used here. The linear response range is of the magnitude of fiber diameter, but it depends on the fiber end distance and the type of the light source.

An possible way to reduce the non-linearity is to use receiving fibers with smaller diameter. But the sensitivity will be also be reduced. By separating the two receiving fiber, the sensitivity can be raised, but the total linear region will be narrowed.

For a silicon diaphragm which is less than or about the dimension of $1\times1\text{mm}^2$, its deflection may be too small to be detected by this kind sensing mechanism, and it is almost impossible to make alignment of fibers on such a diaphragm. For example, for a bossed square diaphragm, dimensions 0.5mm×0.5mm, 3μm thickness, boss side length 500μm, subjected to a pressure change of 0—600mmHg the center deflection is approximately 10 μm[18]. The corresponding response of the optical fiber system used here would be less than 1.

For a silicon diaphragm with dimensions of several millimeters, and several tens of microns thickness, this optical fiber sensor will work very well with satisfactory sensitivity

and linearity. For a 6mm×6mm diaphragm, with 20μm thickness, the total deflection of the diaphragm is 500μm for pressure about 1200mmHg or 160cmH_2O (1.6 bar)[8]. For sensors with similar dimensions, the twin receiving fibers can work very well.

CHAPTER 6

CONCLUSION

A rugged silicon optical fiber sensor has been fabricated utilizing a silicon micro structure created by KOH anisotropical etching. The sensing head of the sensor is a micro machined silicon diaphragm, of which the deflection modulates the intensity of input light signal.

Both theoretical analysis and experimental results demonstrate a satisfactory linearity within a deflection range of the diaphragm from about -100μm to 100μm. The corresponding pressure range depends on the dimension and profile of the diaphragm. The output readings which is the logarithm of the output ratio of two photodiodes are in the range about -10 to 10. With well controlled signal-to-noise ratio, very good sensitivity and resolution can be obtained.

The most striking feature of the sensor is that the output signal is independent on the light source intensity, which means the light source fluctuations can be automatically compensated.

Based on experiments, we can see that the optical fiber sensing mechanism used here is compatible with the well developed silicon micromachining technology, considering the possibility of precision fiber alignment and the compatible linear response range.

It is possible to apply this optical fiber sensing technique to other silicon micro sensors which involve deflections of diaphragms or beams, for example a silicon accelerometer.

APPENDIX A

SIGNAL AMPLIFICATION AND PROCESSING CIRCUIT

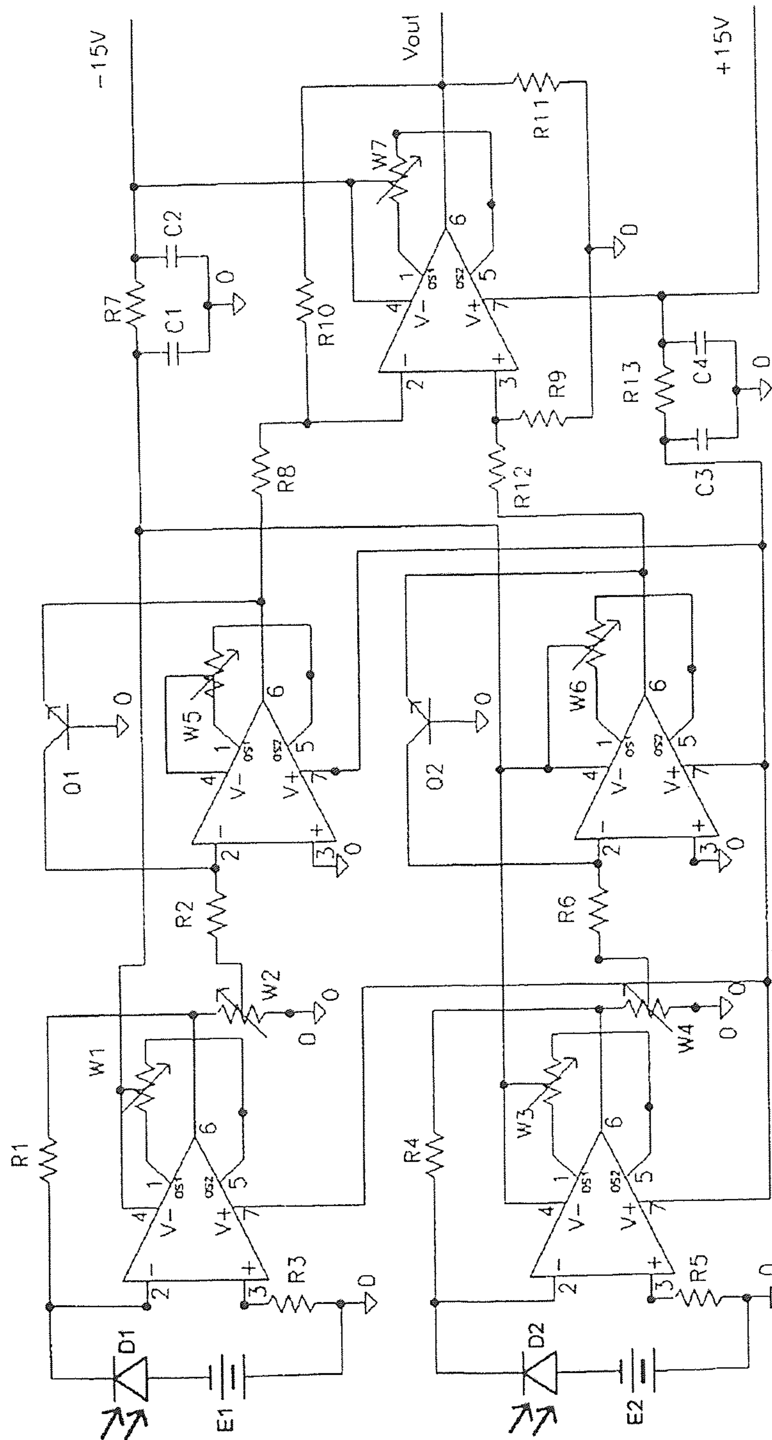

Figure A.1 Signal Amplification and Processing Circuit

APPENDIX B

DATA ACQUISITION AND PROCESSING PROGRAM

```
CLS
OPEN "\DEV\IEEEOUT" FOR OUTPUT AS #1        'Open IEEE488 output path
OPEN "\DEV\IEEEIN" FOR INPUT AS #2          'Open IEEE-488 output path
IOCTL #1, "BREAK"                           'Reset interface
PRINT #1, "RESET"                           'Warm start interface
PRINT #1, "CLEAR"                           'Send device clear
PRINT #1, "REMOTE 24"                       'Put unit 1 in remote
PRINT #1, "REMOTE 25"                       'Put unit 2 in remove
REM **********UNIT 1 SETUP ************************************
PRINT #1, "OUTPUT 24;F0X"                   'DC volts
PRINT #1, "OUTPUT 24;R0X"                   'Auto range
PRINT #1, "OUTPUT 24;P1X"                   'Front panel filter on
PRINT #1, "OUTPUT 24;G1X"                   'Data format, without prefix/suffix
REM *********UNIT 2 SETUP ************************************
PRINT #1, "OUTPUT 25;F0X"                   'DC volts
PRINT #1, "OUTPUT 25;R0X"                   'Auto range
PRINT #1, "OUTPUT 25;P1X"                   'Front panel filter on
PRINT #1, "OUTPUT 25;G1X"                   'Without prefix/suffix
CLS                                         'Clear CRT
REM **********Title Display and Key Board Control********************
LOCATE 10, 10
PRINT CHR$(201);
FOR K = 1 TO 60
PRINT CHR$(205);
NEXT K
PRINT CHR$(187)
FOR K = 11 TO 20
LOCATE K, 10
PRINT CHR$(186)
NEXT K
FOR K = 11 TO 20
LOCATE K, 71
PRINT CHR$(186)
NEXT K
LOCATE 20, 10
PRINT CHR$(200);
FOR K = 1 TO 60
PRINT CHR$(205);
```

```
NEXT K
PRINT CHR$(188)
LOCATE 12, 13
PRINT "          DEPARTMENT OF PHYSICS, NJIT "
PRINT
LOCATE 14, 13
PRINT "        SILICON OPTICAL FIBER PRESSURE SENSOR"
PRINT
LOCATE 18, 13
PRINT "        DATA ACQUISITION AND PROCESSING SYSTEM "
PRINT
LOCATE 22, 28
PRINT "PRESS ANY KEY TO BEGIN."                'Waiting for command
DO WHILE INKEY$ = "": LOOP                     'Waiting for key press
CLS
PRINT "STARTING......."
100 PRINT #1, "ENTER 24"                       'Address Unit 1 to talk
INPUT #2, D                                    'Get Voltage from detector 1
FOR J = 1 TO 1000                              'Delay
NEXT J
PRINT #1, "ENTER 25"                           'Address Unit 2 to talk
INPUT #2, E                                    'Get Voltage from detector 2
FOR J = 1 TO 1000                              'Delay
NEXT J
CLS                                            'Clear CRT
PRINT "DATA1="; D                              'Display Voltage from detector 1
PRINT "DATA2="; E                              'Display Voltage from detector 2
F = D / E                                      'Calculation of voltage ratio
F = LOG(F)                                     'Waiting for key press
IF A$ = "E" OR A$ = "e" THEN 200               'Exit command
GOTO 100
200 CLOSE #1: CLOSE #2
END
```

APPENDIX C

EXPERIMENTAL DATA OF SENSOR TESTING

Table C.1 Experimental Data

Deflection (x10μm)	White Light (output reading)	He-Ne Laser (output reading)	Small gap of Fiber Ends.(Laser) (output reading)	Intensity Reduced (50%) He-Ne Laser (reading)
-24	-6.15			
-22	-6.01			
-20	-5.71	-8.13	-9.28	-9.07
-18	-5.25	-7.71	-9.23	-8.99
-16	-4.70	-7.06	-8.95	-8.77
-14	-4.02	-6.17	-8.21	-8.32
-12	-3.35	-5.44	-7.29	-7.40
-10	-2.71	-4.47	-6.14	-6.14
-8	-2.13	-3.47	-4.74	-5.00
-6	-1.56	-2.51	-3.32	-3.55
-4	-1.02	-1.51	-2.02	-2.20
-2	-0.50	-0.79	-0.94	-1.09
0	0	0	0	0
2	0.52	0.71	0.87	0.77
4	1.00	1.46	1.78	1.66
6	1.52	2.27	2.81	2.70
8	2.07	3.19	4.06	3.85
10	2.58	4.16	5.46	5.26
12	3.16	5.20	6.74	6.60
14	3.75	6.07	7.83	7.72
16	4.35	6.82	8.80	8.70
18	4.95	7.41	9.65	9.61
20	5.50	7.39	10.27	10.23
22	6.03	8.44	10.45	10.31
24	6.50			
26	6.86			

REFERENCES

[1] J. Fraden, *AIP Handbook of Modern Sensors: Physics, Design and Applications,* American Institute of Physics, New York, 1993.

[2] G. Stemme, "Resonant Silicon Sensor," *J. Micromech. Microeng.* vol. 1, pp. 113-125, 1991.

[3] K. M. Mahmoud, R. P. van Kampen, M. J. Rutka and R. F. Wolffendbuttel, *"A Silicon Integrated Smart Pressure Sensor," The 7th International Conference on Sensors,* pp. 217-220, 1993.

[4] W. H. Ko, 'Solid-State Capacitive Pressure Transducers," *Sensors and Transducers,* vol.10, pp. 304-320, 1986.

[5] Y. Zhang and K. D. Wise, "An Ultra-sensitive Capacitive Pressure Sensor with a Bossed Dielectric Diaphragm," *Digest of Solid-State Sensor and Actuator Workshop,* pp. 205-208, June 1994.

[6] L. Christel, K. Petersen, P. Barth, F. Pourahamadi, J. Mallon, Jr. and J. Bryzek, "Single-crystal Silicon Pressure Sensors with 500 × Overpressure Protection, " *Sensors and Actuators*, vol. A21-A23, pp. 84-88, 1990.

[7] J. R. Mallon Jr., F. Pourahmadi, K. Petersen, P. Barth, T. Vermeulen and J. Bryzek, "Low-pressure Sensor Employing Bossed Diaphragms and Precision Etch-Stopping," vol. A21-A23, pp. 89-95, 1990.

[8] J. A. Dziuban, A. Gorecka-Drzazgaand U. Lipowicz, "Silicon Optical Pressure Sensor," *Sensors and Actuators A*, vol.32, pp. 628-631, 1992.

[9] X. Tu and J. N. Zemel, "Vertical-membrane Optical-fiber Pressure Sensor," *Sensor and Actuators A*, vol. 39, pp. 49-54, 1993.

[10] K. E. B. Thornton, D. Uttamchandani and B. Culshaw, "A Sensitive Optically Excited Resonator Pressure Sensor," *Sensors and Actuator A*, vol. 24 , pp. 15-19, 1990.

[11] S. Valette, S. Renard, J. P. Jadot, P. Gidon and C. Erbeia, "Silicon-based Integrated Optics Technology for Optical Sensor Applications," *Sensors and Actuators* , vol. A21-A23, pp. 1087-1091,1990.

[12] K. E. Peterson, "Silicon as a Mechanical Material," *Proceedings of IEEE,* vol.7, pp. 420-457, May,1982.

REFERENCES
(Continued)

[13] M. Di Giovanni, *Flat and Corrugated Diaphragm Design Handbook*, Marcel Dekker Inc., New York, 1982.

[14] H. Chau and K. D. Wise, "Scaling Limits in Batch Fabricated Silicon Pressure Sensors, " *IEEE, Trans. Electron Devices*, vol. ED-34, pp. 851,1987.

[15] Z. Djuric, M. Matic, J. Matovic, R. Petrovic and N. Simicic, "Experimental Determination of Silicon Pressure Sensor Diaphragm Deflection," *Sensors and Actuators A*, vol. 24, pp. 175-179, 1990.

[16] C. J Mullem, K. J. Gabriel, H. Fujita, "Large Deflection Performance of Surface Micromachined Corrugated Diaphragms, " *Digest IEEE transducers '91*, pp. 1014-1017, 1991.

[17] A. Uasukawa, M. Shimazoe, and Y. Matsuoka, "Simulation of Circular Silicon Pressure Sensors With a Center Boss for Very Low Pressure Measurement," *IEEE Transactions on Electron Devices,* vol. 36, No. 7, pp. 1295-1301, July 1989.

[18] Y. Zhang and K. D. Wise, "Performance of Non-planar Silicon Diaphragms Under Large Deflections," *IEEE Micro Electro Mechanical System Workshop* 93, pp. 284-288, 1993.

[19] Y. Zhang, S. B. Crary, and K. D. Wise, "Pressure Sensor Design and Simulation Using the CAEMEMS-D Module," *Digest IEEE Solid-State Sensor and Actuator Workshop*, Hilton Head, South Carolina, pp. 32-35, June 1990.

[20] X. Ding, "Behavior and Application of Silicon Diaphragms with a Boss and Corrugation," *Digest IEEE Solid-State Sensor and Actuator Workshop,* Hilton Head, South Carolina, pp. 166-169, June 1992.

[21] J. Jerman, "The Fabrication and Use of Micromachined Corrugated Silicon Diaphragms," *Sensors and Actuators,* vol. A21-A23, pp. 988-992, 1990.

[22] R. H.. Johnson, S. Karbassi, U. Sridhar and B. Spelrich, "A High Sensitivity Ribbed and Bossed Pressure Transducer," *Sensors and Actuators A*, vol. 35, pp.93-99, 1992.

[23] L. Yuan and J. Pan, "Fiber-optic Temperature Sensor with Variable-sensitivity," *SPIE's Internationals Symposium on Optical Tools for Manufacturing and Advanced Automation*, Vol. 2070, pp. 7-10, Sep. 1993.

[24] L. Yuan, J. Pan, T. Yang and G. Han, "Analysis of the Compensation Mechanism of a Fiber-optic Displacement Sensor," *Sensors and Actuators* A, vol. 36, pp. 177-182, 1993.

REFERENCES
(Continued)

[25] S. M. Sze, *Semiconductor Devices, Physics and Technology*, John Wiley and Sons, New York, 1985.

[26] S. M. Sze, *VLSI Technology*, McGraw-Hill Book Company, New York, 1983.

[27] H. Seidel, L. Csepregi, A. Heuberger and H. Baumgartel, "Anisotropic Etching of Crystalline Silicon in Alkaline Solutions," *J. Electrochem. Soc.*, vol. 137, No.11, pp. 3613-3612, 1990.